© 2014. Published by The Company of Biologists Ltd | Journal of Cell Science (2014) 127, 686–699 doi:10.1242/jcs.145037

RESEARCH ARTICLE

RalA promotes a direct exocyst–Par6 interaction to regulate polarity in neuronal development

Amlan Das[1,*], Sangeetha Gajendra[2,*], Katarzyna Falenta[2,*], Madeleine J. Oudin[2], Pascal Peschard[3], Shanshan Feng[1], Bin Wu[1], Christopher J. Marshall[3], Patrick Doherty[2], Wei Guo[1,‡] and Giovanna Lalli[2,‡]

ABSTRACT

Cell polarization is essential for neuronal development in both the embryonic and postnatal brain. Here, using primary cultures, *in vivo* postnatal electroporation and conditional genetic ablation, we show that the Ras-like small GTPase RalA and its effector, the exocyst, regulate the morphology and polarized migration of neural progenitors derived from the subventricular zone, a major neurogenic niche in the postnatal brain. Active RalA promotes the direct binding between the exocyst subunit Exo84 and the PDZ domain of Par6 through a non-canonical PDZ-binding motif. Blocking the Exo84–Par6 interaction impairs polarization in postnatal neural progenitors and cultured embryonic neurons. Our results provide the first *in vivo* characterization of RalA function in the mammalian brain and highlight a novel molecular mechanism for cell polarization. Given that the exocyst and the Par complex are conserved in many tissues, the functional significance of their interaction and its regulation by RalA are likely to be important in a wide range of polarization events.

KEY WORDS: Ral, Exocyst, Par6, Neuroblast migration, Neuronal polarity

INTRODUCTION

Cell polarization is a key event in neuronal development, controlling neurogenesis (Farkas and Huttner, 2008), neuronal migration and synaptogenesis (Solecki et al., 2006; Valiente and Marín, 2010). Proper localization of polarity determinants, directed vesicle traffic, and regulated cytoskeletal dynamics are required for polarization in many cell types, including neurons and neural progenitors. Small GTPases coordinate these events to establish cell polarity in response to intra- and extracellular cues (Mellman and Nelson, 2008; McCaffrey and Macara, 2009; Hall and Lalli, 2010). Among these, the Ras-like GTPase Ral, of which there are two isoforms, RalA and RalB, has emerged as an important polarity regulator in a variety of contexts, including basolateral membrane trafficking and tight junction formation in epithelial cells (Shipitsin and Feig, 2004; Hazelett et al., 2011), polarized migration of fibroblasts and cancer cells (Rossé et al., 2006; Spiczka and Yeaman, 2008) and tumorigenesis (Camonis and White, 2005; Lim et al., 2005; Oxford et al., 2005; Bodemann and White, 2008; Hazelett and Yeaman, 2012). During brain development, Ral is involved in asymmetric division of neuroblasts (Carmena et al., 2011), neuronal migration in the neocortex (Jossin and Cooper, 2011), neurite branching (Lalli and Hall, 2005) and activity-dependent spine growth (Teodoro et al., 2013). RalA also regulates axon initiation in cortical neurons by promoting an interaction between one of its effectors, the exocyst, and the partitioning-defective (Par) Par3–Par6–aPKC (atypical protein kinase C) complex (Lalli, 2009), an evolutionarily conserved master regulator of polarity (Goldstein and Macara, 2007). Despite their importance, the underlying molecular mechanisms by which RalA exerts its regulatory function are still unclear.

The exocyst is an evolutionarily conserved octameric protein complex consisting of Sec3, Sec5, Sec6, Sec8, Sec10, Sec15, Exo70 and Exo84 (TerBush and Novick, 1995; Hsu et al., 1996; TerBush et al., 1996; Guo et al., 1999). Assembly of the exocyst complex mediates vesicle targeting and tethering at the plasma membrane for exocytosis (Hsu et al., 2004; Munson and Novick, 2006; He and Guo, 2009). Inhibiting exocyst function disrupts polarization in different contexts, including localized exocytosis in *Saccharomyces cerevisiae* (He and Guo, 2009), basolateral protein delivery in epithelial cells (Grindstaff et al., 1998), ciliogenesis (Zuo et al., 2009; Feng et al., 2012), and neurite outgrowth and branching (Vega and Hsu, 2001; Murthy et al., 2003; Lalli and Hall, 2005). Notably, the exocyst can co-immunoprecipitate with Par complex components and together they can regulate cell motility (Rosse et al., 2009), axon specification (Lalli, 2009) and ciliogenesis (Zuo et al., 2009). However, the molecular mechanisms of this interaction remain unknown.

Active Ral regulates exocyst assembly by directly binding to Sec5 and Exo84 (Moskalenko et al., 2002; Sugihara et al., 2002; Moskalenko et al., 2003) to control migration, membrane traffic, and cytoskeletal dynamics (Hertzog and Chavrier, 2011; Liu and Guo, 2012). These processes also play a fundamental role in neurogenesis, which persists in the postnatal brain in two niches, the dentate gyrus of the hippocampus and the subventricular zone (SVZ) (Zhao et al., 2008). SVZ stem cells generate neuroblasts that move rostrally, forming the 'rostral migratory stream' (RMS), towards the olfactory bulb (OB), where they differentiate into inhibitory interneurons (Luskin, 1993; Lois and Alvarez-Buylla, 1994; Doetsch and Alvarez-Buylla, 1996; Lledo et al., 2006). This polarized migration is crucial for postnatal neurogenesis, controlling the fate and integration of new neurons into a pre-existing synaptic network (Belvindrah et al., 2011).

Here, we describe a role for RalA and the exocyst in SVZ-derived neuroblast polarity and migration by using RMS explants, *in vivo* postnatal electroporation of RalA mutants and genetic

[1]University of Pennsylvania Department of Biology, Philadelphia, PA 19104, USA. [2]Wolfson Centre for Age-Related Diseases, King's College London, Guy's Campus, London SE1 1UL, UK. [3]The Institute of Cancer Research, Division of Cancer Cell Biology, Chester Beatty Laboratories, 237 Fulham Road, London SW3 6JB, UK.

*These authors contributed equally to this work

‡Authors for correspondence (giovanna.lalli@kcl.ac.uk; guowei@sas.upenn.edu)

Received 23 October 2013; Accepted 5 November 2013

Journal of Cell Science

Journal of Cell Science (2014) 127, 686–699 doi:10.1242/jcs.145037

deletion of *Rala*. We uncover a mechanism in which active RalA promotes the direct binding between Exo84 and Par6. Disrupting this interaction impairs polarity in postnatal migratory neuroblasts and embryonic neurons.

RESULTS

RalA depletion inhibits RMS neuroblast migration

RalA regulates neurite branching and neuronal polarization in embryonic neurons (Lalli and Hall, 2005; Lalli, 2009). We found a punctate distribution of RalA in postnatal SVZ-derived rat migratory neuroblasts (Fig. 1A; supplementary material Fig. S1A,B). We inhibited RalA expression in these cells using a validated siRNA approach (Lalli and Hall, 2005; Lalli, 2009). Neuroblasts display a 50–70% decrease in RalA levels 48–72 hours after nucleofection with a siRNA oligonucleotide compared to control siRNA-nucleofected cells (supplementary material Fig. S1A–D). RalA depletion did not cause an increase in apoptosis, as shown by similarly low levels of cleaved caspase 3 positivity in control and RalA siRNA-nucleofected cells (supplementary material Fig. S1E). Given the involvement of Ral in cell motility (Oxford et al., 2005; Rossé et al., 2006; Spiczka and Yeaman, 2008), we examined whether its depletion affects neuroblast migration using 3D culture in Matrigel, a system recapitulating the neuroblast mode of migration observed *in vivo* (Wichterle et al., 1997). Given that the most effective RalA depletion was observed between 48 and 72 hours after siRNA nucleofection, we re-aggregated neuroblasts co-nucleofected with GFP and control or RalA siRNA oligonucleotides in hanging drops over 5 hours,

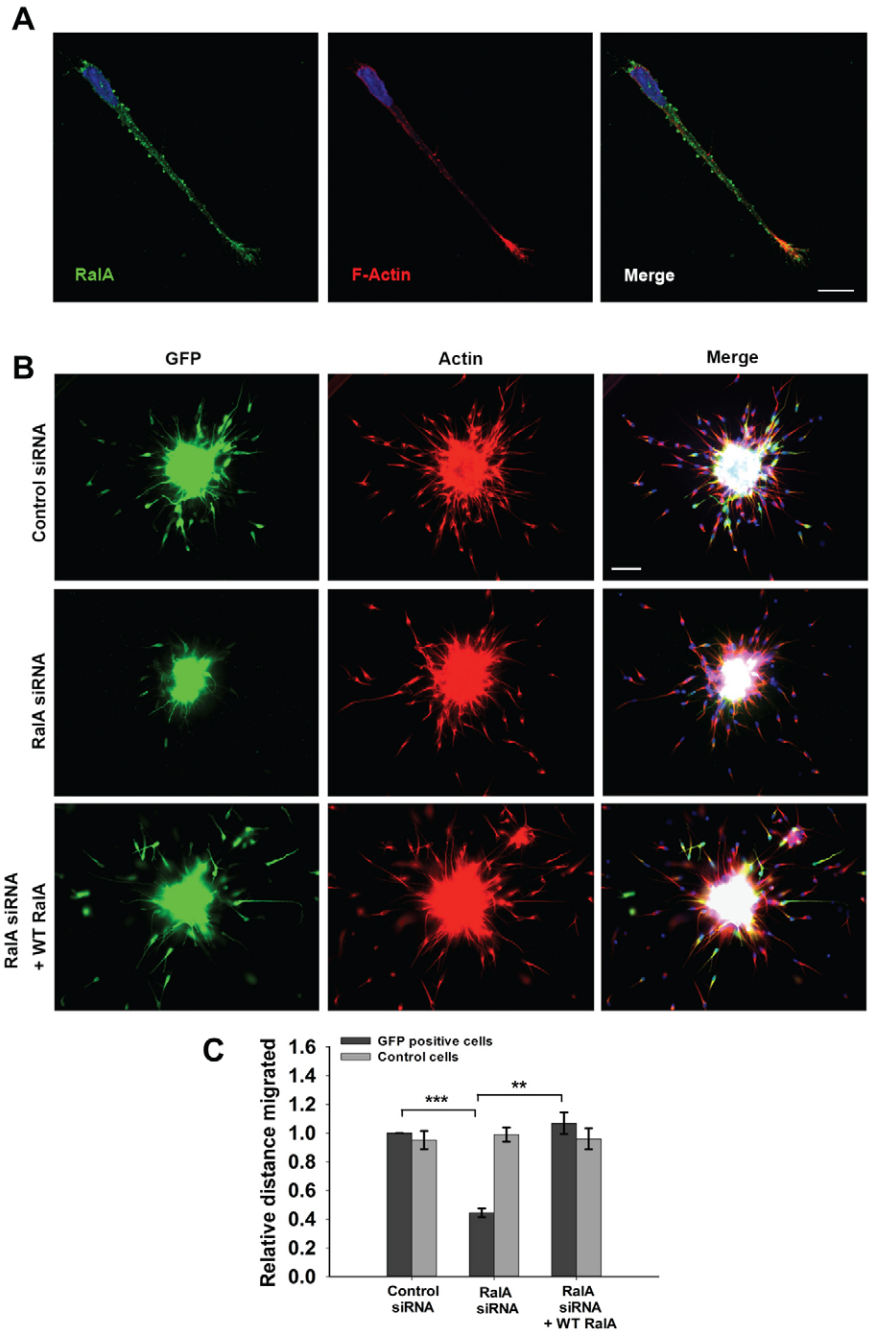

Fig. 1. RalA depletion impairs RMS neuroblast migration *in vitro*. (A) Confocal images of a rat RMS neuroblast embedded in Matrigel and stained for RalA (green) and F-actin (red). The cell nucleus (blue) is visualized by Hoechst. Scale bar: 10 μm. (B) Rat RMS neuroblasts were nucleofected with control siRNA + GFP, RalA siRNA + GFP, or RalA siRNA + pCAG-WTRalA-IRES-EGFP (encoding an siRNA-resistant WT RalA version), embedded in Matrigel 48 hours after nucleofection, and left to migrate for 24 hours before immunostaining for GFP (green) and incubation with fluorescent phalloidin (red). Cell nuclei are stained with Hoechst (blue). Representative images showing nucleofected (green) and non-nucleofected (red only) neuroblasts. Scale bar: 50 μm. (C) Migration distance was quantified for both transfected (GFP-positive) and non-transfected (control) neuroblasts. Inhibition of migration by RalA siRNA is rescued by siRNA-resistant WT RalA. Neuroblasts nucleofected with a control siRNA oligonucleotide migrate a similar distance to non-nucleofected cells. Results are mean ± s.e.m. $^{**}P<0.01$; $^{***}P<0.001$ ($n=3$ independent experiments). See also supplementary material Figs S1 and S2.

Journal of Cell Science (2014) 127, 686–699 doi:10.1242/jcs.145037

cultured them in suspension for 48 hours, embedded them in Matrigel and let them migrate for 24 hours before fixation (Falenta et al., 2013). RalA knockdown caused a ~60% reduction in migration (Fig. 1B,C). Control cells in the same aggregates (GFP-negative, stained in red for F-actin) migrated to a similar extent in all conditions (Fig. 1B, middle column, and Fig. 1C). Co-nucleofection of a plasmid encoding a siRNA-resistant wild-type (WT) RalA and GFP restored migration to control levels, showing the specificity of the RalA siRNA effect (Fig. 1B, bottom row, and Fig. 1C).

During neuroblast migration, nucleokinesis follows the extension of a leading process (Schaar and McConnell, 2005). Quantitative tracking analysis from time-lapse imaging over a 4-hour period (supplementary material Fig. S2A) showed a substantial reduction in migrated distance and speed for RalA-depleted neuroblasts (supplementary material Fig. S2B,C). RalA-depleted cells extended dynamic leading processes that frequently retracted, impairing nucleokinesis. Control nuclei displayed large saltatory movements (jumps >5 µm) (supplementary material Fig. S2D), consistent with previous observations (Schaar and McConnell, 2005; Oudin et al., 2011). RalA depletion caused a ~6-fold reduction in the percentage of large nucleokinetic jumps, which were largely replaced by small oscillations (supplementary material Fig. S2D,E). Thus, RalA might be involved in regulating neuroblast migration.

Perturbing RalA activity affects the orientation and morphology of RMS neuroblasts *in vivo*

To assess the role of RalA in RMS neuroblasts in the intact brain, we altered RalA activity by *in vivo* postnatal electroporation of Myc-tagged RalA versions – wild type (WT), dominant-negative (DN, RalAS28N), constitutively active (CA, RalAQ72L) and 'fast cycling' (between the GDP- and GTP-bound state; FC, RalAF39L) (Lalli, 2009) cloned into pCAG-IRES-EGFP (Niwa et al., 1991; Causeret et al., 2009). The empty vector (EV), or pCX-EGFP (Oudin et al., 2011) served as controls. Electroporation in the lateral ventricle of P2 mouse pups allows transfection of a neuroblast subpopulation in the intact SVZ (Boutin et al., 2008; Sonego et al., 2013a). Brains were immunostained for GFP 5 days later to examine SVZ-derived neuroblasts in the RMS. Co-expression of Myc-tagged RalA and GFP was confirmed by immunostaining (data not shown). Over 95% of neuroblasts expressing WT, CA or FC RalA extended their leading process towards the OB, similar to control cells expressing only GFP (Fig. 2A). Instead, neuroblasts expressing DN RalA displayed a ~25% shorter leading process, with over a 3-fold increase in the percentage of cells oriented away from the OB (Fig. 2B,C). Both CA and FC RalA significantly increased process length (Fig. 2B), consistent with the idea that active RalA elicits protrusion extension.

To analyze how the different RalA variants affected migration, we counted the number of labelled cells in three different regions along the rostrocaudal axis of the RMS 5 days after electroporation: the descending arm (area 1), the horizontal arm (area 2) and the core of the OB (area 3) (Fig. 2D). Expression of DN RalA caused a ~50% increase in the percentage of cells found in area 2, suggesting disrupted migration dynamics (Fig. 2E). On average, we observed similar amounts of GFP, CA or DN RalA-expressing cells along the entire RMS (data not shown), consistent with a lack of effect on cell viability. Taken together, these results suggest that RalA activity regulates the morphology and polarity of RMS neuroblasts *in vivo*.

Deletion of *Rala* affects neuroblast orientation and morphology *in vivo*

We further investigated the role of RalA in RMS neuroblasts using a RalA conditional knockout model based on the Cre-lox system ($Rala^{lox/lox}$), because *Rala* null mice are embryonic lethal (Peschard et al., 2012). We electroporated $Rala^{lox/lox}$mice with pCAG-Cre-IRES2-EGFP, allowing simultaneous expression of Cre recombinase and GFP (Woodhead et al., 2006), to genetically delete *Rala* in a subset of RMS neuroblasts in an otherwise wild-type (wt) environment. Brain slices were stained for GFP 5 days after electroporation (Fig. 3A,B). Cre expression alone did not affect neuroblast migration in wt mice (supplementary material Fig. S3A). As expected, expressing only GFP (by electroporating pCX-EGFP) in $Rala^{lox/lox}$ animals did not affect neuroblast morphology, polarity or migration (supplementary material Fig. S3B,C), ruling out any abnormalities due to genetic background. To monitor RalA expression, we immunostained $Rala^{lox/lox}$ neuroblasts transfected with pCAG-Cre-IRES2-EGFP for RalA. Visible reduction of RalA expression [46.70%±4.0 (±s.e.m.) decrease in RalA fluorescence intensity levels in GFP-positive cells compared to untransfected neuroblasts; $P<0.001$, $n=25$ GFP-positive and 25 GFP-negative cells] was only detected 5 days after Cre transfection (Fig. S3D), when neuroblasts have already started to reach the OB. At this time point, deletion of *Rala* altered neuroblast morphology, causing a ~25% decrease in leading process length and a significant increase in cells lacking a process (Fig. 3C,D). In addition, we observed a >6-fold increase in the amount of misoriented neuroblasts compared to wt animals (Fig. 3E). There was no significant difference in the number of cells reaching the OB, possibly owing to a long half-life of RalA *in vivo* and/or to the time necessary to achieve full Cre expression and function (unpublished data). To test the function of the related RalB isoform on RMS neuroblast morphology and migration, we electroporated pCX-EGFP in $Rala^{lox/lox}$; $Ralb^{-/-}$ mice (Peschard et al., 2012). Lack of RalB did not cause detectable changes in neuroblast morphology, orientation or migration (Fig. 3). These results support the conclusion that RalA, but not RalB, is required for proper morphology and orientation of neuroblasts *in vivo*.

RalA controls neuroblast migration through the exocyst complex

Expression of either CA or FC RalA increased elongation of the leading process (Fig. 2), similar to active RalA-enhanced axon extension involving the exocyst (Lalli and Hall, 2005). To determine whether RalA regulates neuroblast morphology and migration through the exocyst, we electroporated CA RalA or an Exo84-uncoupled CA RalA version (RalAQ72LA48W) (Fukai et al., 2003; Hazelett et al., 2011) and examined RMS neuroblasts 5 days later. To assess the specificity of the effects caused by Exo84-uncoupled RalA, we also electroporated CA RalA uncoupled from RalBP1 (RalAQ72LD49N), another Ral effector (Jullien-Flores et al., 2000; Lalli and Hall, 2005) (Fig. 4A). Although all RalA mutants increased process length (Fig. 4B), only Exo84-uncoupled RalA (A48W) caused a substantial increase in the proportion of cells lacking a leading process (Fig. 4C), and significantly increased the number of misoriented neuroblasts (Fig. 4D). Electroporation of another RalA mutant uncoupled from both Sec5 and Exo84 (RalAQ72LD49E) (Moskalenko et al., 2003) similarly increased the percentage of misoriented neuroblasts (10.18%±2.62; $P<0.01$; $n=5$ brains), reinforcing the role of the exocyst in regulating neuroblast polarity downstream of RalA. Uncoupling

Journal of Cell Science (2014) 127, 686–699 doi:10.1242/jcs.145037

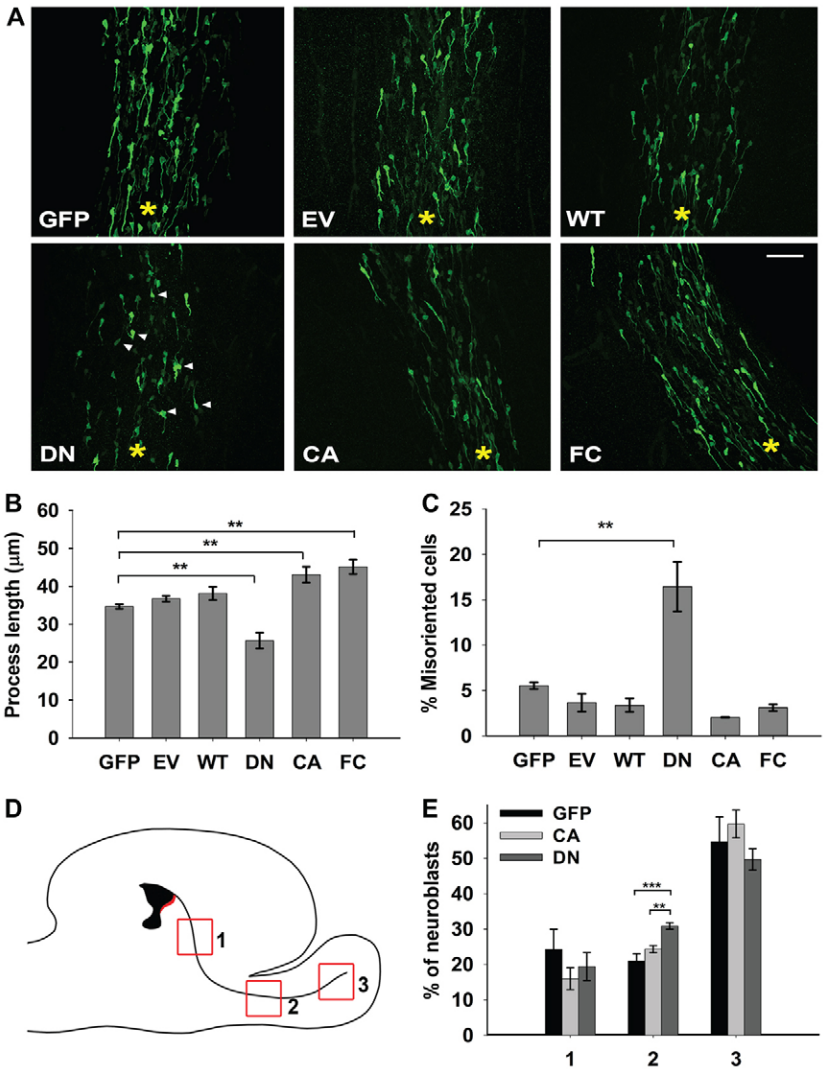

Fig. 2. RalA regulates neuroblast morphology and directionality *in vivo*. (A) P2 mice were electroporated with pCX-EGFP (GFP) or one of these pCAG-IRES-EGFP constructs: empty vector (EV), wild-type (WT) RalA, dominant-negative (DN) RalA, constitutively active (CA) RalA, or fast cycling (FC) RalA. After 5 days, brains were sliced and immunostained for GFP. Representative confocal projections of sagittal RMS sections. Yellow asterisks indicate the relative position of the OB. Expression of DN RalA visibly disrupts neuroblast morphology and orientation (white arrowheads), whereas in all other cases most neuroblasts extend a leading process towards the OB. Scale bar: 50 μm. (B) DN RalA significantly reduces process length, whereas expression of CA or FC RalA slightly increases it. (C) Only DN RalA disrupts the orientation of neuroblasts towards the OB. (D) Schematic diagram indicating the RMS and OB areas considered for migration analysis (area 1, descending RMS; area 2, horizontal RMS; area 3, OB core). (E) Expression of DN RalA causes accumulation of cells in region 2. Results are mean ± s.e.m. $^{**}P<0.01$, $^{***}P<0.001$ (between three and eight brains were analyzed for each electroporated construct).

RalA from Exo84 also impaired migration, causing a ~30% decrease in the proportion of cells found in the OB compared to both CA and RalBP1-uncoupled RalA (Fig. 4E). To assess the longer-term consequences of this effect, we analysed the distribution of GFP-positive cells found in the OB 14 days after *in vivo* electroporation. At this later time point, most of the control cells have radially migrated in the OB (Fig. 5A) and started to differentiate into interneurons. About 75% of control GFP-labelled cells were found in the outer OB (Fig. 5A–C, area B) whereas ~25% were in the OB core (Fig. 5A–C, area A). Expression of CA RalA led to a ~15% decrease in the proportion of cells found in the outer OB, whereas expression of Exo84-uncoupled RalA caused a more pronounced effect (~35% decrease) (Fig. 5C). Uncoupling RalA from Exo84 therefore affects neuroblast polarity, morphology and migration, ultimately disrupting the normal distribution of newborn neurons in the OB.

Given that the interaction between the exocyst and the Par complex contributes to different polarization events (Lalli, 2009; Zuo et al., 2009), we asked whether a similar interaction could also be detected in RMS lysates, which are positive for the migrating neuroblast marker doublecortin (Dcx) (Koizumi et al., 2006) (Fig. 5D). An anti-Sec6 antibody immunoprecipitated not only the other exocyst subunits Sec8 and Exo84 but also Par3, supporting the presence of an endogenous exocyst–Par interaction in the RMS (Fig. 5D).

Active RalA promotes a direct interaction between Exo84 and Par6

We investigated the molecular mechanism underlying the exocyst–Par interaction by testing whether exocyst subunits can directly bind a Par complex component. We first examined Exo84, a direct binding partner of active RalA (Moskalenko et al., 2003), and potentially of Par3 and Par6 because of a putative canonical PDZ-binding motif present at the C-terminus of Exo84, which could bind the PDZ domains of Par3 and Par6 (Joberty et al., 2000). Rat Exo84 was translated *in vitro* in the presence of [^{35}S]methionine and incubated with different GST-tagged PDZ domains of Par3 and Par6 [Par3-PDZ1, Par3-PDZ2, Par3-PDZ3, Par3-PDZ(2+3) and Par6-PDZ] (Lin et al., 2000). Exo84 specifically bound to GST–Par6-PDZ (Fig. 6A). This interaction was confirmed with a GST pull-down assay using hTERT-RPE1 cell lysates, where endogenous Exo84 bound to GST-Par6-PDZ (Fig. 6B).

To examine whether Exo84 mediates the interaction between Par6 and the exocyst, a GST pull-down assay was carried out in hTERT-RPE1 cells transfected with Exo84 siRNA. We found that Exo84 levels decreased by almost 90%, whereas the levels of

Journal of Cell Science (2014) 127, 686–699 doi:10.1242/jcs.145037

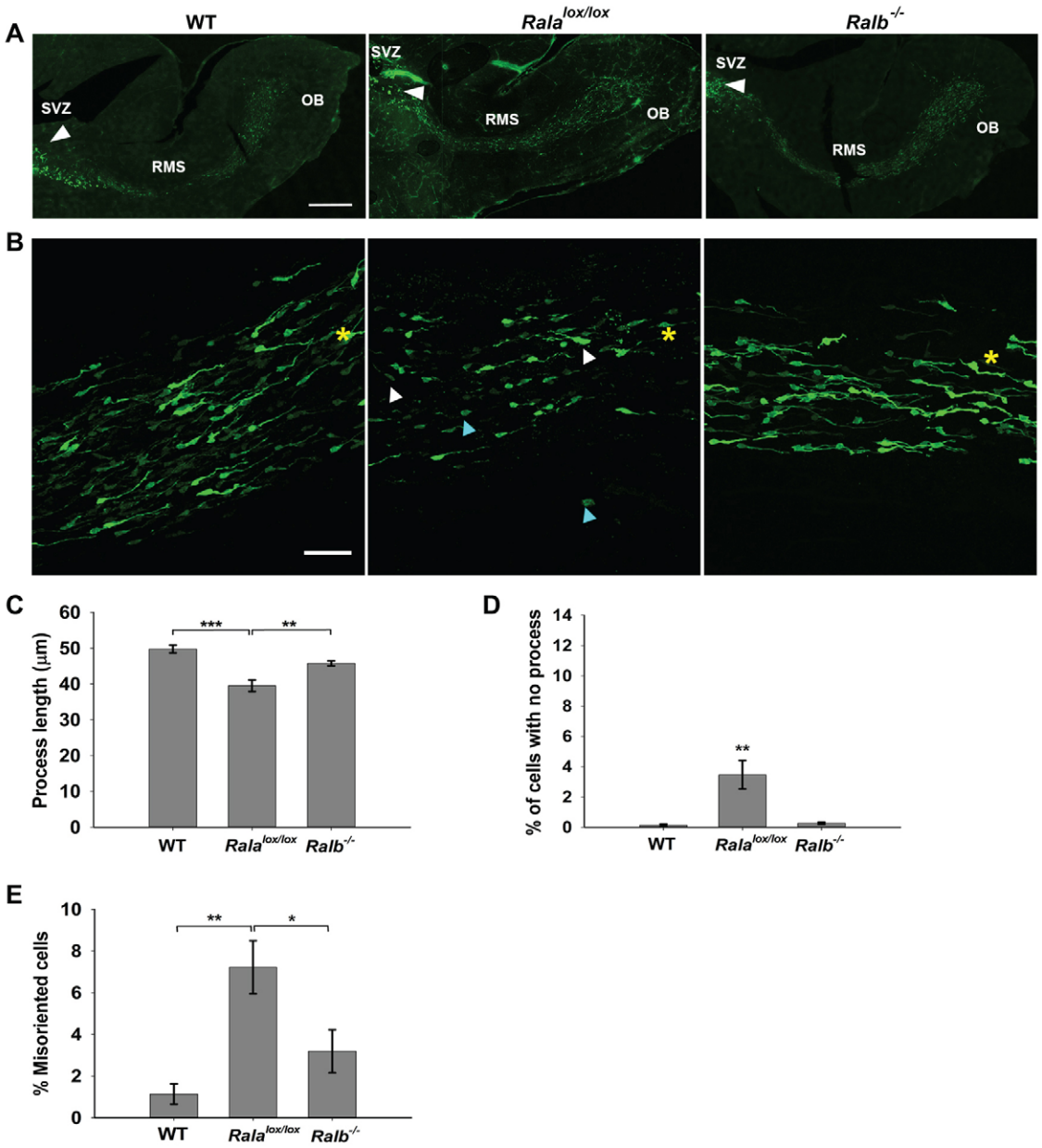

Fig. 3. Genetic deletion of *Rala*, but not *Ralb* disrupts neuroblast morphology and orientation. (A) pCAG-Cre-IRES2-EGFP was electroporated in WT and *Rala*$^{lox/lox}$ mice, and pCX-EGFP was electroporated in *Rala*$^{lox/lox}$; *Ralb*$^{-/-}$ mice. After 5 days, brain slices were prepared and stained for GFP. Representative confocal projections of sagittal brain slices showing overall labeling along the RMS. White arrowheads indicate the injection site. Scale bar: 500 μm. (B) Representative confocal projections of RMS neuroblasts expressing Cre/GFP in WT, *Rala*$^{lox/lox}$ and GFP in *Rala*$^{lox/lox}$;*Ralb*$^{-/-}$ mice. Yellow asterisks indicate the relative position of the OB. White arrowheads indicate neuroblasts oriented away from the OB; blue arrowheads indicate neuroblasts lacking a leading process. Scale bar: 50 μm. Genetic deletion of *Rala* significantly reduces process length (C), and increases the percentage of neuroblasts without a leading process (D) or oriented away from the OB (E), whereas genetic deletion of *Ralb* has no significant effect. Results are mean ± s.e.m. **P*<0.05; ***P*<0.01; ****P*<0.001 (*n*=4 brains for WT, *n*=5 brains for *Rala*$^{lox/lox}$, *n*=6 brains for *Rala*$^{lox/lox}$;*Ralb*$^{-/-}$). See also supplementary material Fig. S3.

another exocyst subunit, Sec8, remained unchanged (Fig. 6C). In control cells, GST–Par6-PDZ precipitated both Exo84 and Sec8. Exo84 depletion abolished the ability of Par6-PDZ to bind Sec8. In contrast, depleting Sec8 did not affect binding of Exo84 to Par6-PDZ. Importantly, the Par6-PDZ–Exo84 interaction was substantially reduced in RalA-depleted cells (Fig. 6D). Given that RalA activity modulates the exocyst–Par association (Lalli, 2009), we tested whether RalA regulates the direct interaction between Exo84 and Par6. The presence of constitutively active RalA (RalA23V) enhanced the binding between Exo84 and Par6 by ~50% compared to control samples, whereas dominant-negative RalA (RalA28N) did not affect the Exo84–Par6 interaction (Fig. 6E,F).

Exo84 binds to Par6 through a non-canonical PDZ-binding motif

Besides a classical C-terminal PDZ-binding domain, Exo84 also contains an internal PDZ-binding motif (E^{345}GAVDLLD^{352}) located close to the Ral-binding domain (Fig. 7A). This non-canonical PDZ-binding sequence is also found in Pals1, another polarity regulator interacting with Par6-PDZ (Penkert et al.,

Journal of Cell Science (2014) 127, 686–699 doi:10.1242/jcs.145037

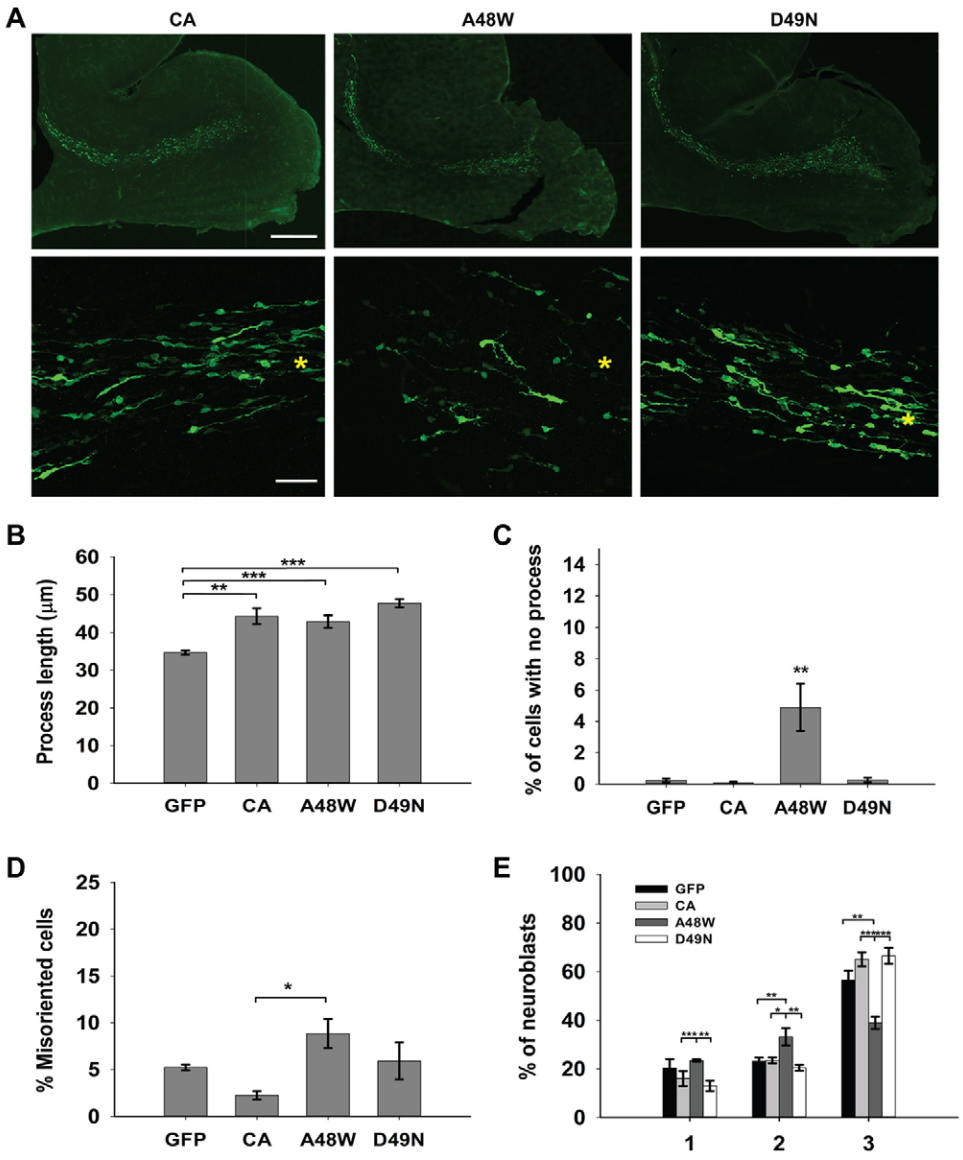

Fig. 4. RalA regulates neuroblast morphology and migration through the exocyst complex. (A) P2 mice were electroporated with pCX-EGFP or pCAG-IRES-EGFP vectors encoding CA RalA, CA RalA uncoupled from Exo84 (A48W) or from RalBP1 (D49N). After 5 days, brain slices were immunostained for GFP. Top row: representative confocal projections of sagittal slices showing overall labeling along the RMS. Scale bar: 500 μm. Bottom row: representative confocal projections of RMS sections. Asterisks indicate relative position of the OB. Expression of CA RalA A48W visibly disrupts neuroblast morphology and orientation. Scale bar: 50 μm. All constructs increased process length (B), but only the A48W mutant significantly increased the percentage of cells lacking a process (C), altered orientation (D), and delayed migration (E), increasing cells in regions 1–2 and decreasing cells in region 3. Results are mean ± s.e.m. $^{*}P<0.05$; $^{**}P<0.01$; $^{***}P<0.001$ ($n=6$ brains for each electroporated construct).

2004). We therefore translated full-length (FL) Exo84 *in vitro* and Exo84 mutants lacking either the C-terminal PDZ-binding motif (CΔ3) or harboring mutations in the internal motif at two key residues crucial for PDZ binding (INT-mt; $V^{348}D^{349}\rightarrow A^{348}A^{349}$). These Exo84 variants were subjected to a GST pull-down assay with recombinant GST–Par6-PDZ. Both Exo84FL and CΔ3 bound to Par6, whereas Exo84INT-mt failed to bind to GST–Par6-PDZ, suggesting that the interaction between the Par6-PDZ and Exo84 is mediated by the internal PDZ-binding motif of Exo84 (Fig. 7B). Similar results were obtained by a GST pull-down assay using recombinant GST–Par6-PDZ and cell lysates from hTERT-RPE1 cells expressing different GFP-tagged Exo84 proteins (Fig. 7C). As a control, we confirmed that mutating the internal PDZ-binding domain of Exo84 did not affect its ability to bind one of its known interacting partners, Exo70 (Fig. 7D). We also examined the ability of Exo84FL, Exo84INT-mt and Exo84CΔ3 to bind Par6-PDZ in the presence of active RalA. Whereas Exo84FL and Exo84CΔ3 interacted with GST–Par6-PDZ, Exo84INT-mt remained unable to bind Par6-PDZ (supplementary material Fig. S4A).

To test whether the interaction between the non-canonical PDZ-binding motif of Exo84 and Par6-PDZ is direct, we expressed a His_6-tagged Exo84 fragment (INT-frag, aa 251–450) containing the internal PDZ-binding motif from bacteria. Recombinant GST or GST–Par6-PDZ was incubated with a His_6-tagged Exo84 INT-frag or Exo84 INT-frag harboring the $V^{348}D^{349}\rightarrow A^{348}A^{349}$ mutations (INT-frag-mt, aa 251–450). Exo84 INT-frag was sufficient to interact with GST–Par6-PDZ, whereas Exo84 INT-frag-mt lost its ability to bind GST–Par6-PDZ (Fig. 7E). Overexpression of a GFP-tagged Exo84 INT-frag decreased the endogenous exocyst–Par interaction in primary cortical neurons (Fig. 7F). Taken together, these results show that Exo84 directly interacts with Par6-PDZ through its non-canonical PDZ-binding motif, and that residues 348 and 349 are crucial for this interaction.

Disrupting the Exo84–Par6 interaction affects neuroblast morphology and polarity

We asked whether the Exo84–Par6 interaction regulates neuroblast morphology, polarity and migration. RMS neuroblasts were

Journal of Cell Science (2014) 127, 686–699 doi:10.1242/jcs.145037

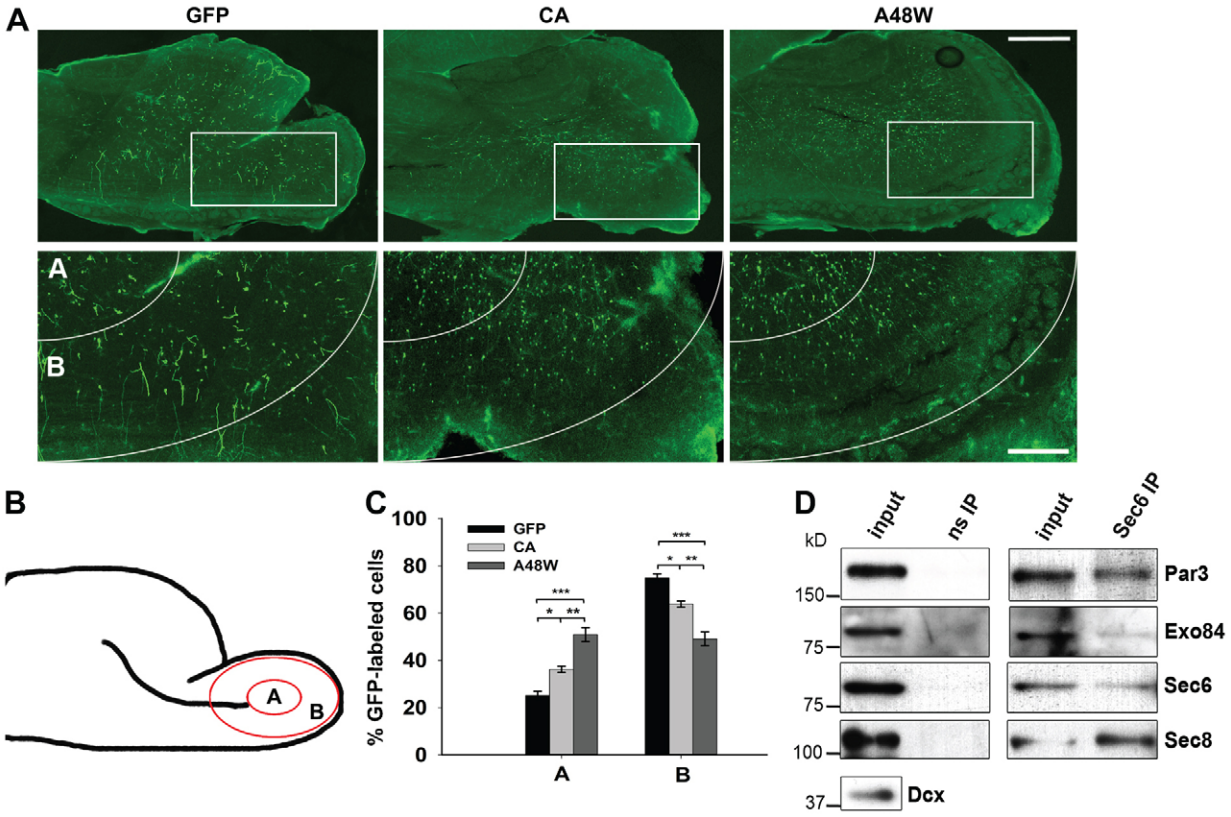

Fig. 5. Uncoupling RalA from Exo84 affects newborn neuron distribution in the OB. (A) P2 mice were electroporated with either pCX-EGFP or pCAG-IRES-EGFP vectors encoding CA RalA or CA RalA A48W. After 14 days, brain slices were prepared and stained for GFP. Top row: representative confocal projections from sagittal brain slices showing overall labeling in the OB. Scale bar: 500 μm. Bottom row: high magnification of the OB insets overlaid with the mask used for quantification (A, inner OB; B, outer OB). Expression of CA RalA A48W visibly affects the distribution of newborn neurons in the OB. Scale bar: 250 μm. (B) Schematic diagram indicating the OB areas considered for quantitative analysis. (C) CA RalA A48W caused a significant cell accumulation in the inner OB, whereas CA RalA had a more modest effect. Results are mean ± s.e.m. *$P<0.05$; **$P<0.01$; ***$P<0.001$ ($n=4$ brains for GFP and CA RalA, $n=5$ brains for CA RalA A48W). (D) An anti-Sec6 antibody co-immunoprecipitates Sec8, Exo84 and Par3 from P7 rat RMS lysates positive for the migrating neuroblast marker doublecortin (Dcx). A non-specific mouse IgG (ns) was used as a negative control.

nucleofected with GFP, GFP-tagged Exo84 INT-frag or INT-frag-mt. Cells were re-aggregated in clusters, embedded in Matrigel 24 hours after nucleofection and left to migrate for 24 hours. Expression of Exo84 INT-frag caused a ~40% decrease in migration distance, whereas Exo84 INT-frag-mt caused a more modest inhibitory effect (Fig. 8A,B). Overexpression of Exo84 INT-frag, but not INT-frag-mt also significantly impaired axon specification in embryonic cortical neurons, a process relying on the exocyst–Par interaction (Lalli, 2009) (supplementary material Fig. S4B,C).

To test the functional role of the exocyst–Par interaction *in vivo*, a pCAG-IRES-EGFP vector expressing Exo84 INT-frag or INT-frag-mt was electroporated in mouse pups. Brains were collected 5 days later and stained for GFP. Expression of Exo84 INT-frag visibly altered the morphology of migrating neuroblasts, many of which displayed ectopic branching (Fig. 8C). Whereas Exo84 INT-frag and INT-frag-mt slightly increased process length (Fig. 8D), only Exo84 INT-frag caused a ~4-fold increase in the amount of misoriented cells (Fig. 8E) and significantly increased the percentage of branched cells compared to GFP-expressing control neuroblasts (Fig. 8F). Similar relative percentages of cells were detected in areas 1–3 of the RMS 5 days after electroporation of all three constructs (data not shown). Taken together, these results point to a crucial functional role for the Exo84–Par6 interaction in the regulation of neuroblast morphology and polarity.

DISCUSSION

We have uncovered a role for the small GTPase RalA and the exocyst complex in the regulation of neural progenitor polarity using primary cultures, *in vivo* electroporation of RalA mutants and, for the first time, inducible genetic deletion of *Rala* in the brain. Our study highlights a novel molecular mechanism controlling cell polarity. By binding to its effector Exo84, RalA promotes the direct interaction between Exo84 and the PDZ domain of Par6 through an internal non-canonical PDZ-binding motif. A functional role for this interaction was further demonstrated in the polarization of postnatal migrating neuroblasts and embryonic neurons.

Modulation of RalA activity is important for proper neuroblast morphology and polarity *in vivo*, as shown by the disruption of these features in neuroblasts expressing inactive RalA. We could not properly assess the effect of *Rala* genetic deletion on migration because a substantial decrease of RalA protein levels was only observed at 5 days after Cre transfection, when most of the electroporated neuroblasts had already migrated along the RMS. This delay might be due to the time required for Cre-mediated excision but also suggests that RalA has a prolonged

Journal of Cell Science (2014) 127, 686–699 doi:10.1242/jcs.145037

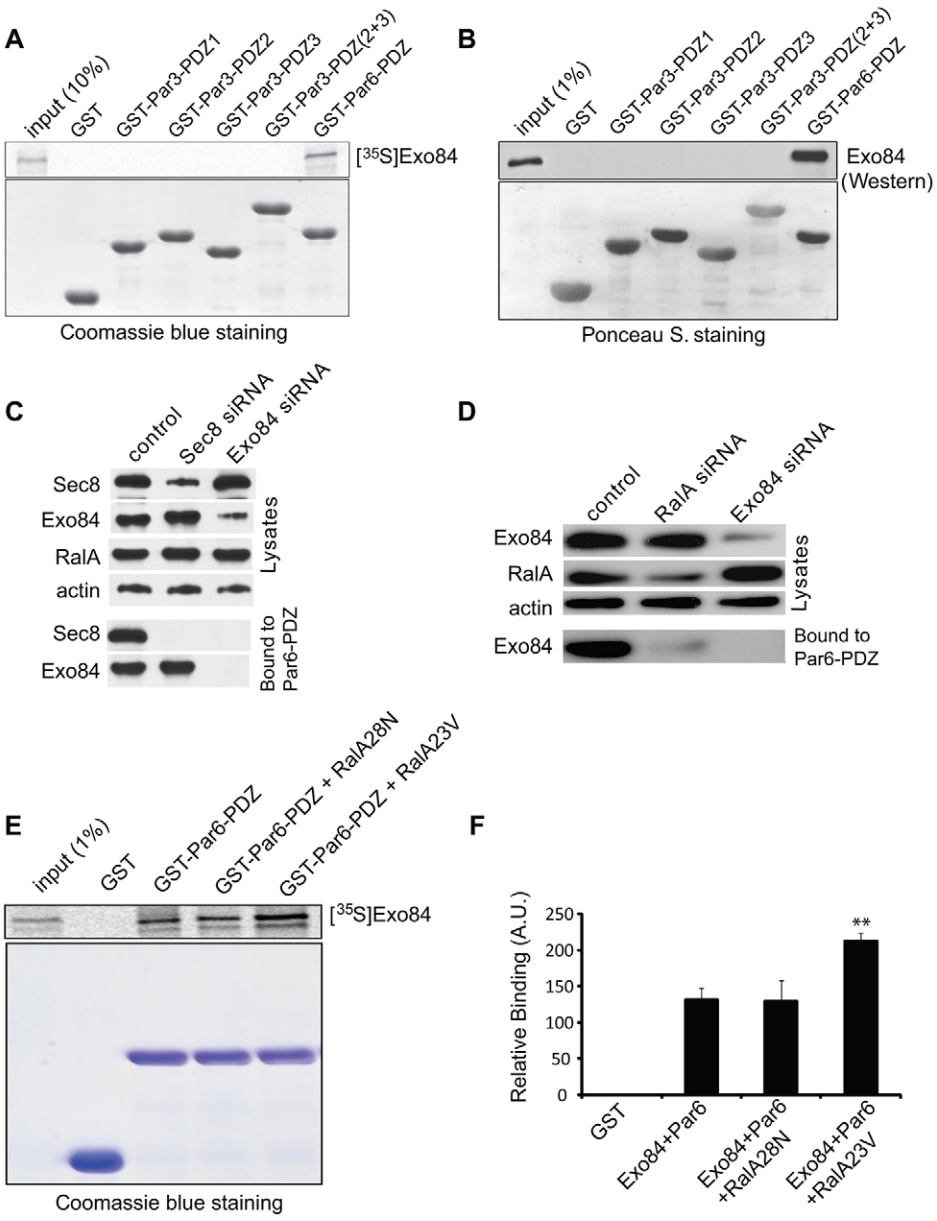

Fig. 6. Active RalA promotes an interaction between Exo84 and Par6. (A) GST-tagged PDZ domains of Par3 and Par6 were incubated with *in vitro* translated Exo84. Only GST–Par6-PDZ bound Exo84. (B) GST–Par6-PDZ but not the GST-PDZ domains of Par3 pulled down endogenous Exo84 from hTERT-RPE1 cell lysates. (C) Knockdown of Exo84 diminished the interaction between Par6 and the exocyst. Top panel: western blot of lysates from hTERT-RPE1 cells transfected with Luciferase (control), Sec8 or Exo84 siRNA showing effective reduction of the respective proteins. Bottom panel: in control cells GST–Par6-PDZ precipitated endogenous Sec8 and Exo84. GST–Par6-PDZ still interacted with Exo84 after Sec8 knockdown. When Exo84 was knocked down, neither Exo84 nor Sec8 were detected in the GST–Par6-PDZ precipitate, suggesting that Exo84 mediates the interaction of the exocyst with the PDZ domain of Par6. (D) Knockdown of RalA inhibited Par6-exocyst binding. Top panel: western blot of lysates from hTERT-RPE1 cells transfected with Luciferase (control), RalA or Exo84 siRNA showing effective reduction of the respective proteins. Bottom panel: in control cells GST–Par6-PDZ precipitated endogenous Exo84. When RalA was knocked down, less Exo84 bound to GST–Par6-PDZ. (E) RalA enhanced binding between Exo84 and Par6-PDZ. *In vitro* translated radiolabeled Exo84 was incubated with GST–Par6-PDZ with or without constitutively active (RalA23V) or dominant-negative RalA (RalA28N). (F) Quantification of Exo84-Par6 binding shown in E. Results are mean ± s.e.m. $^{**}P<0.01$ ($n=3$ independent experiments).

half-life in neuroblasts *in vivo* and that reduced levels are sufficient for normal motility. Moreover, compensatory mechanisms might act *in vivo* following *Rala* loss. Still, downregulation of RalA in *Rala*$^{lox/lox}$ mice significantly disrupted neuroblast morphology and polarity, whereas genetic deletion of *Ralb* did not have any significant effect (Fig. 3), indicating some different roles between the two Ral isoforms, which can act redundantly in other systems (Lalli and Hall, 2005; Peschard et al., 2012). This evidence, together with the defects caused by siRNA-mediated RalA depletion *in vitro* and by expression of inactive or exocyst-uncoupled RalA mutants *in vivo*, strongly supports a role for this small GTPase in regulating neuroblast morphology and polarity. This might have important implications for the maturation of neuroblasts into neurons (Belvindrah et al., 2011; Sanai et al., 2011) and for their ability to re-route to injured brain areas (Arvidsson et al., 2002; Sundholm-Peters et al., 2005). Potential modulators of RalA activity in migrating neuroblasts could be cell adhesion molecules, such as N-cadherin or integrins, which are enriched in the RMS (Yagita et al., 2009; Kazanis et al., 2010) and have been linked to RalA activation in other systems (Lalli and Hall, 2005; Jossin and Cooper, 2011). Another interesting candidate is cannabinoid signaling, which we have recently identified as a major regulator of neural progenitor migration *in vivo* (Oudin et al., 2011) and has been associated with RalA in pathways controlling neurite outgrowth (He et al., 2005).

The exocyst is a crucial RalA effector in neuroblast migration, as shown by the delayed migration of neuroblasts expressing Exo84-uncoupled RalA, not only along the RMS, but also at later stages in the OB, where neuroblasts migrate radially and differentiate. Indeed, perturbing the RalA–Exo84 interaction significantly disrupted the final distribution of newborn neurons in the OB (Fig. 5), which is likely to affect their fate and synaptic integration, as in the case of another migration regulator, doublecortin (Belvindrah et al., 2011). RMS neuroblast migration is saltatory, alternating process extension with

Journal of Cell Science (2014) 127, 686–699 doi:10.1242/jcs.145037

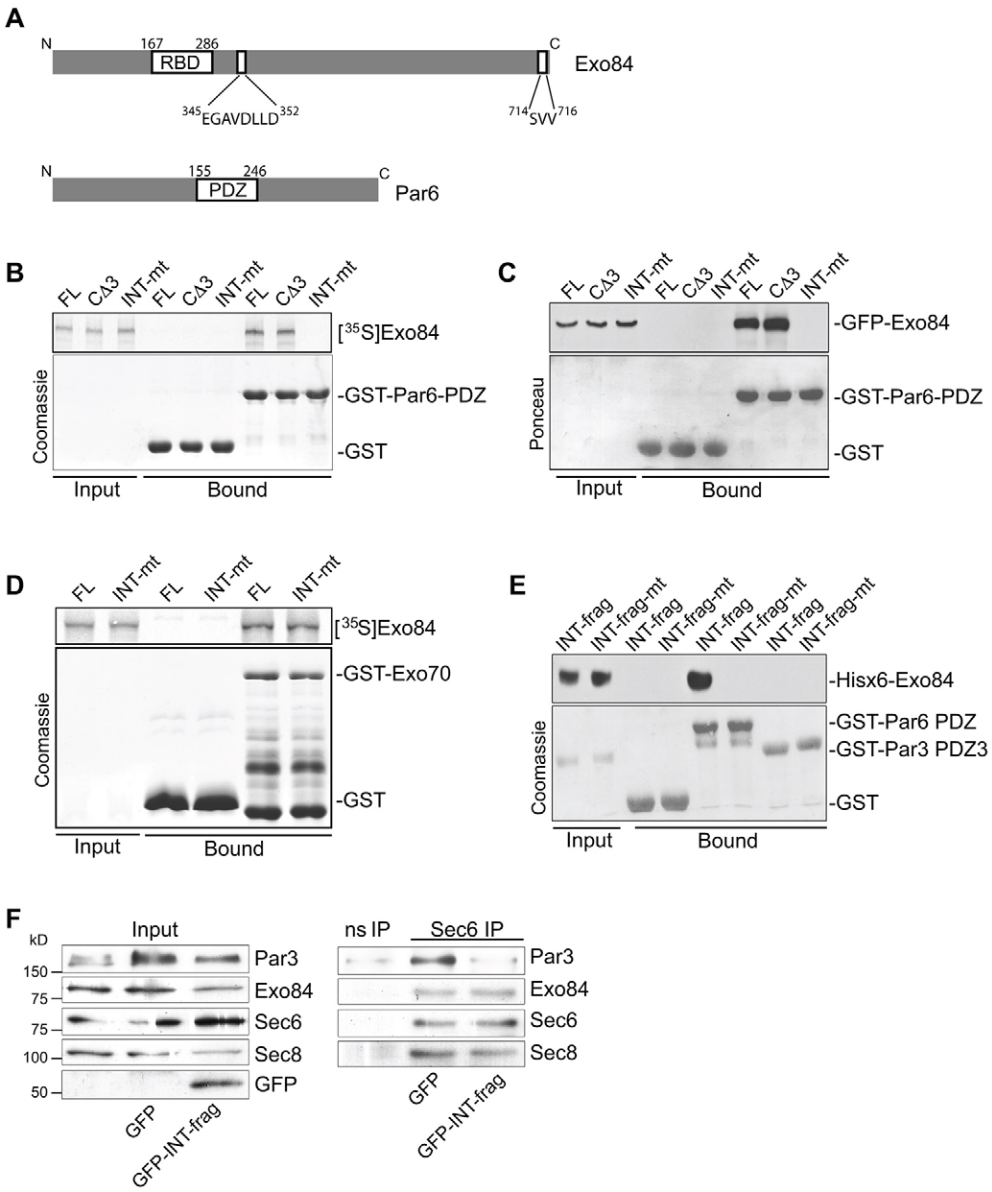

Fig. 7. Exo84 interacts with Par6 by a novel PDZ-binding motif. (A) Domain structure of Exo84 and Par6. Exo84 has a canonical PDZ-binding motif at the C-terminus ($S^{174}VV^{176}$) and a non-canonical PDZ binding motif ($E^{345}GAVDLLD^{352}$) located downstream of the Ral-binding domain (RBD). (B) *In vitro* translated full-length radiolabeled Exo84 (FL), Exo84CΔ3 (lacking the C-terminal PDZ-binding domain) and Exo84INT-mt (harboring the $V^{348}D^{349}$→AA mutations in the internal PDZ-binding motif) were incubated with GST–Par6-PDZ. Mutating the non-canonical PDZ-binding domain of Exo84 abolished interaction with Par6-PDZ. (C) hTERT-RPE1 cells were transfected with pEGFPC2-Exo84FL, pEGFPC2-Exo84CΔ3 and pEGFPC2-Exo84INT-mt. After 2 days, cells lysates were incubated with GST or GST–Par6-PDZ. GST–Par6-PDZ pulled down Exo84 and Exo84CΔ3 but not Exo84INT-mt as detected by western blot with an anti-GFP antibody. (D) The Exo84 PDZ-binding motif is dispensable for exocyst association. *In vitro* translated radiolabeled Exo84FL and INT-mt bound equally well to GST-tagged Exo70. (E) The non-canonical PDZ-binding motif of Exo84 directly binds Par6-PDZ. GST or GST–Par6-PDZ were incubated with a purified His_6-tagged Exo84 internal fragment comprising the non-canonical PDZ domain (aa 251–450, INT-frag) or the same Exo84 fragment harboring the $V^{348}D^{349}$→AA mutations (INT-frag-mt). Bound Exo84 proteins were detected by western blot using an anti-His_6 antibody. Mutating the two residues of the Exo84 internal fragment abolished binding to Par6-PDZ. See also supplementary material Fig. S4. (F) Overexpression of Exo84 INT-frag in primary cortical neurons disrupted the endogenous exocyst–Par interaction, as shown by the decreased amount of Par3 co-immunoprecipitated by an anti-Sec6 antibody compared to GFP expression. A non-specific mouse IgG (ns) was used as a negative control.

nucleokinesis, with a very dynamic leading protrusion (Nam et al., 2007; Sonego et al., 2013b). Interestingly, perturbing the RalA–Exo84 interaction impaired neuroblast migration, and caused both process loss and misorientation. These observations suggest that the RalA–exocyst interaction might be involved in multiple functions during neuroblast migration, such as process initiation and orientation in response to extracellular stimuli along the RMS (Lalli, 2013).

RalA and the exocyst are involved in neuronal migration in the developing neocortex (Letinic et al., 2009; Jossin and Cooper, 2011). At the molecular level, however, the consequence of RalA–exocyst interaction is still unclear. Our work has now

Journal of Cell Science (2014) 127, 686–699 doi:10.1242/jcs.145037

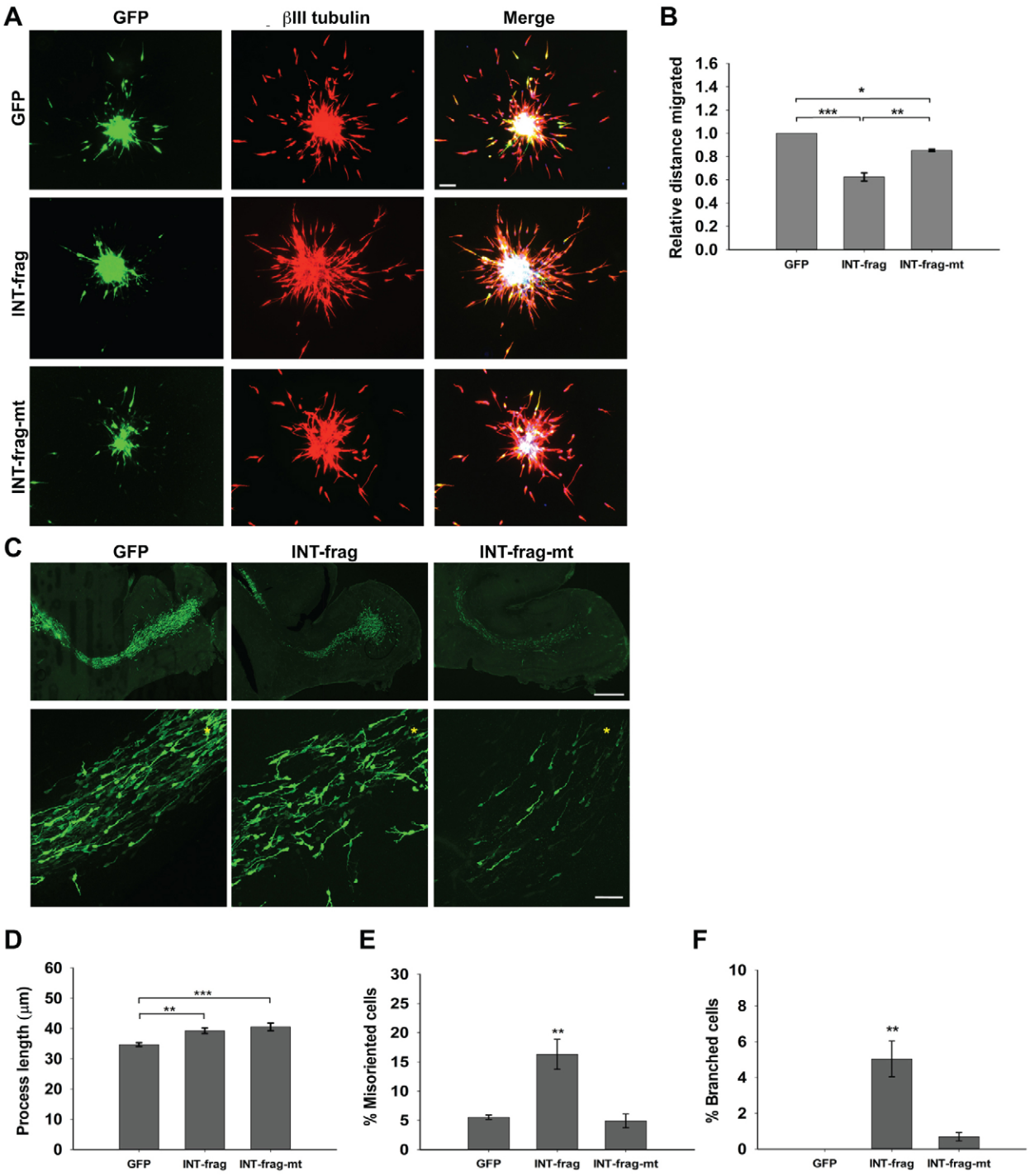

Fig. 8. Disrupting the Exo84–Par6 interaction affects neuroblast morphology, migration and polarity. (A) Rat neuroblasts were nucleofected with plasmids encoding GFP, and GFP-tagged Exo84 INT-frag or Exo84 INT-frag-mt. After 1 day, cells were embedded in Matrigel and left to migrate for 24 hours before immunostaining for anti-βIII tubulin (red). Expression of GFP–Exo84 INT-frag visibly impaired migration. Scale bar: 100 μm. (B) Expression of Exo84 INT-frag and Exo84 INT-frag-mt caused a ~40% and 15% decrease in migration distance, respectively. Results are mean ± s.e.m. *$P<0.05$; **$P<0.01$; ***$P<0.001$ ($n=3$ independent experiments). (C) Mice were electroporated with pCX-EGFP and pCAG-IRES-EGFP encoding Exo84 INT-frag or INT-frag-mt. After 5 days, brain slices were stained for GFP. Top row: representative confocal projections from sagittal slices showing overall labeling along the RMS. Scale bar: 500 μm. Bottom row: representative RMS confocal projections. Asterisks indicate relative position of the OB. Scale bar: 50 μm. Expression of Exo84 INT-frag visibly disrupted neuroblast morphology, slightly increasing process length (D), and significantly increasing the percentage of misoriented (E) and branched neuroblasts (F). Expression of Exo84 INT-frag-mt slightly increased process length, but did not affect branching nor orientation. Results are mean ± s.e.m. **$P<0.01$; ***$P<0.001$ ($n=6$ brains for GFP and Exo84 INT-frag, $n=5$ brains for Exo84 INT-frag-mt).

Journal of Cell Science (2014) 127, 686–699 doi:10.1242/jcs.145037

shown that active RalA promotes the interaction between the exocyst subunit Exo84 and the Par complex component Par6. Like the polarity protein Pals1, Exo84 binds the PDZ domain of Par6 through an internal, non-canonical PDZ-binding motif. Importantly, expression of this Exo84 internal fragment disrupts the exocyst–Par interaction and affects neuroblast morphology and orientation to a similar extent to *Rala* genetic deletion or Exo84-uncoupling of RalA. Expression of the same Exo84 fragment also impairs axon specification in polarizing cortical neurons, a process relying on a RalA-modulated interaction between the exocyst and the Par complex (Lalli, 2009). Furthermore, mutating two crucial residues in the internal PDZ-binding motif of Exo84 abolishes the disrupting effect, supporting the functional importance of this region in cell polarization. Given that the Exo84 Ral-binding domain is located close to the internal PDZ-binding motif, binding of active RalA could cause a conformational change in Exo84 to enhance its interaction with Par6-PDZ.

In epithelial cysts and neuronal progenitors, Par6 is recruited to the cortex by active Cdc42, which binds to its CRIB domain (Joberty et al., 2000; Chen et al., 2006). Interestingly, binding of Pals1 with Par6-PDZ occurs independently of Cdc42 binding to Par6 (Penkert et al., 2004). Localized recruitment of Par6 can occur independently of Cdc42, as reported in dendritic spines (Zhang and Macara, 2008). Future studies are needed to address a potential link between RalA and Cdc42 in migrating neuroblasts and in polarizing neurons, given the similar localization of both GTPases at the nascent axon tip (Schwamborn and Püschel, 2004; Lalli, 2009).

Expressing the Exo84 PDZ-binding motif did not disrupt migration as did Exo84-uncoupled RalA. This might seem surprising; however, based on our data the Exo84 internal PDZ-binding motif is not required for exocyst complex association. In the RMS, RalA-promoted exocyst assembly might serve multiple functions, such as the polarized delivery of integrins (Spiczka and Yeaman, 2008) and matrix metalloproteinases (Liu et al., 2009), which can regulate migration along the RMS (Murase and Horwitz, 2002; Belvindrah et al., 2007; Bovetti et al., 2007), and the recruitment of IQGAP1 (Sakurai-Yageta et al., 2008), a signaling scaffold protein involved in neuroblast migration (Balenci et al., 2007). In addition, our single-end-point assay in fixed brain slices, which can detect strong migration phenotypes, might lack the sensitivity needed to uncover subtler defects in cell dynamics. Future studies using live imaging of brain slice cultures will help address this point.

In summary, we have uncovered a novel signaling mechanism involving RalA, Exo84 and Par6 for the control of cell polarity. Although our study focuses on the RalA-promoted exocyst–Par interaction in a neuronal context, it is likely that such a regulatory mechanism operates in other polarization events, such as the establishment of epithelial asymmetry, directed cell migration or immune synapse formation (Grindstaff et al., 1998; Ludford-Menting et al., 2005; Hertzog and Chavrier, 2011).

MATERIALS AND METHODS

Antibodies and reagents

Antibodies used were: mouse anti-Sec6 and anti-tau-1 (Calbiochem), mouse anti-RalA and anti-Sec8 (BD Biosciences), rabbit anti-Par3 (Upstate), rabbit anti-cleaved caspase 3 (Cell Signaling), rabbit anti-GFP (Invitrogen), mouse anti-GFP (Proteintech), mouse anti-Myc (Abcam). Mouse anti-Sec8 and anti-Exo84 were gifts from Shu-Chan Hsu (Rutgers University, Piscataway, NJ). Alexa-Fluor-488- and Texas-Red-conjugated secondary antibodies and Texas-Red–phalloidin were from Invitrogen. HRP-conjugated antibodies were from Dako. Cell culture reagents were from Invitrogen and all other reagents were from Sigma unless otherwise specified.

Animals

All procedures were performed in accordance with UK Home Office regulations (Animals Scientific Procedures Act, 1986). P2–P3 CD1 mouse pups were obtained from Charles River. P5–P7 Sprague Dawley rat pups were obtained from Harlan. The generation of $Rala^{lox/lox}$ and $Rala^{lox/lox}$; $Ralb^{-/-}$ mice in FVB background was as previously described (Peschard et al., 2012).

In vivo postnatal electroporation

Electroporation was performed in P2 mice as previously described (Oudin et al., 2011). Animals were subjected to five electrical pulses of 100 V for 50 milliseconds with 850-millisecond intervals using a CUY21SC electroporator (Nepagene) (Sonego et al., 2013a).

Embryonic cortical neuron cultures

E18 cortical neurons were nucleofected and cultured as described previously (Lalli, 2009). Neurons extending single processes that were at least twice as long as other neurites and tau-1-positive were scored as polarized. At least 110 cells were analyzed for every nucleofected construct in each of three independent experiments.

RMS neuroblast culture

The RMS was dissected from P5–P7 mice or rats (Oudin et al., 2011). Following brief trituration, cells were re-suspended in pre-equilibrated Neurobasal complete medium (containing B27 supplement, 2 mM L-glutamine and 0.6% glucose) or nucleofected (see below). Cells were plated onto polyornithine- and laminin-coated 6-well plates (1×10^6 cells/well) and maintained in Neurobasal complete medium at 37℃ under 5% CO_2. Reaggregated nucleofected neuroblasts were embedded in Matrigel as previously described (Oudin et al., 2011).

Neuroblast nucleofection

Dissociated RMS neuroblasts were resuspended in mouse/rat neuron nucleofection solution (Lonza) according to the manufacturer's instructions. Each sample was mixed with 3 µg DNA or 9 µg siRNA, and nucleofected using program G-013. For western blot analysis, cells were plated onto polyornithine- and laminin-coated six-well plates (1×10^6 cells/well). For migration assays, cells were re-suspended in 30 µl of DMEM + 10% FCS, pipetted as a drop inside a p35 dish lid, and inverted over a dish containing Neurobasal complete medium. Hanging drops were transferred into the medium 5 hours later and cultured in suspension for 48 hours before embedding in growth-factor-reduced Phenol-Red-free Matrigel (BD) on glass coverslips (Falenta et al., 2013). Neuroblasts were allowed to migrate for 24 hours in Neurobasal complete medium at 37℃ under 5% CO_2 before fixation.

Immunocytochemistry

Matrigel-embedded neuroblasts were fixed in 4% PFA for 40 minutes, washed with PBS, blocked and permeabilized with 15% goat serum, 0.3% Triton X-100, 0.1% BSA in phosphate-buffered saline (PBS) for 1 hour at room temperature. Primary antibodies were diluted in the same solution and incubated overnight at 4℃. Coverslips were washed, incubated with secondary antibodies plus Hoechst 33342 for 2 hours at room temperature and mounted with mounting medium (Dako).

Immunohistochemistry

Electroporated brains were hemisected, fixed in 4% PFA overnight at 4℃, embedded in 15% gelatin, and left for 1 hour at room temperature followed by 2 hours at 4℃. After fixing in 4% PFA overnight at 4℃, they were cut on a Vibratome (Leica) into 75-µm-thick sagittal sections. Slices were blocked and permeabilized for 1 hour at room temperature in 1% BSA, 0.1% Triton X-100, 0.1% sodium azide in PBS and incubated overnight at 4℃ with primary antibodies diluted in the same solution. After washing in PBS, slices were incubated with secondary antibodies

Journal of Cell Science (2014) 127, 686–699 doi:10.1242/jcs.145037

for 3 hours, washed in PBS and mounted. *z*-stacks (images taken every 0.5–1.5 µm) of the RMS were captured on a Zeiss LSM 710 confocal microscope using EC Plan Neofluar 10× 0.3 NA and 40× 1.3 NA objectives and Zeiss Zen software. All images were digitally processed in Photoshop, and where needed the brightness and contrast features were modified for the entire field of view to better visualize cell morphology.

Analysis of neuroblast morphology and migration in fixed brain slices

The morphology of GFP-expressing neuroblasts was examined from confocal *z*-stack projections of 75-µm-thick sagittal brain slices immunostained with an anti-GFP antibody. Process length was measured as the distance from the base of the cell body to the tip of the leading process using ImageJ. Cells were considered lacking a process if they did not display any visible protrusion extending from the cell soma, or branched if they displayed one or more primary and/or secondary branches from the leading process. To analyze orientation, we traced a line in the middle of the cell body running perpendicular to the direction of migration along the RMS towards the OB. Neuroblasts with their leading process extending in the sector opposite to the direction of migration were considered misoriented. At least 250 cells were analyzed from each brain, and between three and six brains were analyzed for each electroporated construct or genotype.

To analyze migration 5 days after electroporation, the RMS was classified into three anatomically distinct areas (area 1, descending arm of the RMS; area 2, RMS horizontal arm; area 3, core of the OB) as previously described (Belvindrah et al., 2011). Projections of confocal *z*-stacks were used to count the number of GFP-labeled neuroblasts in areas 1–3 in all slices containing the RMS (typically four slices per brain). The percentage of cells in each area (relative to the total number of labeled cells along the entire RMS) was calculated for statistical comparison among samples. Between three and eight brains were analyzed per genotype or electroporated construct.

To analyze the distribution of GFP-labeled cells in the OB, a mask outlining the inner ('A') and outer ('B') OB areas (minor axis, 1.25 and 3 mm; major axis, 0.73 and 1.7 mm, respectively) was aligned with the edge of the OB on confocal projections of sagittal brain slices (Fig. 5B). For each brain, the percentage of cells in the two OB areas was calculated after counting GFP-positive cells in all the slices containing the OB (typically five slices per brain).

Analysis of migration in fixed neuroblast aggregates

Images of immunostained aggregates were captured on a Zeiss Axioplan 2 microscope equipped with an ApoTome module and a Zeiss MRm Axiocam CCD camera using A-Plan 5× 0.12 NA, A-Plan 10× 0.25 NA and Plan Apo 20× 0.75 NA objectives and Axiovision software. The distance from the edge of an aggregate to the furthest migrated neuroblast perpendicular to the edge was measured at six points around the entire periphery of the aggregate using ImageJ. For each experiment 10 to 20 isolated aggregates were analyzed.

Tracking analysis

For time-lapse imaging, nucleofected and re-aggregated neuroblasts were embedded in Matrigel in a 4-chamber 35-mm Hi-Q4 culture dish (Nikon) and imaged in Neurobasal complete medium. Images were captured by the Nikon Biostation IM software using a Nikon Biostation (an automatic multipoint time-lapse imaging system with controlled environment maintained at 37℃ under 5% CO_2) with a 20× 0.8 NA objective every 3 minutes for 24 hours. Tracking analysis was performed using Volocity software (Perkin Elmer) as previously described (Oudin et al., 2011), and limited to the first 7 hours of filming. Neuroblasts emerged from aggregates at different times during the filming period, and cells were tracked for their first 4 hours of migration upon exiting aggregates. At least 40 cells were tracked for each condition in each experiment.

In vitro binding experiments

Rat Exo84 was subcloned in pcDNA3.1 and *in vitro* translated with the TNT quick-coupled system (Promega) in the presence of [^{35}S]methionine. A total of 5 µl of the TNT reaction mixture was incubated with 10 µg bacterially purified PDZ domains of Par3 and Par6 in 0.5 ml of binding buffer (50 mM Tris-HCl pH 7.4, 150 mM NaCl, 1 mM EDTA, 2 mM $MgCl_2$, 1% Triton X-100) for 2 hours at 4℃. After four washes with binding buffer, bound Exo84 was analyzed by SDS-PAGE and autoradiography. In some cases *in vitro* translated Exo84 was incubated with 1 µg of either purified RalA23V or RalA28N in 0.1 ml of buffer (20 mM Tris-HCl pH 7.4, 100 mM NaCl, 5 mM EDTA, 1 mM dithiothreitol (DTT) and 10 mM $MgCl_2$) for 1 hour at 25℃ before adding purified Par3 or Par6 PDZ domains. For GST–PDZ pull-down assays, hTERT-RPE1 cells were lysed in a buffer containing 20 mM Tris-HCl pH 7.5, 25 mM KCl, 1 mM $MgCl_2$, 0.5 mM EGTA, 1 mM DTT, 0.5% Triton X-100 and protease inhibitors. The cell lysate (1 mg of total protein) was mixed with 20 µl (50% v/v) of glutathione–Sepharose conjugated with 10 µg of GST–Par3 or –Par6 PDZ domains for 2 hours at 4℃. Beads were then washed five times with lysis buffer. Bound Exo84, Sec8 and RalA were monitored by western blotting. For binding experiments with recombinant fusion proteins, bacterially purified GST-tagged PDZ domains and His_6-tagged Exo84 proteins were incubated in binding buffer (50 mM Tris-HCl pH 7.4, 150 mM NaCl, 1 mM EDTA, 2 mM $MgCl_2$, 1% Triton X-100) for 2 hours at 4℃. After four washes with binding buffer, bound Exo84 was analyzed by SDS-PAGE and western blotting.

Statistical analysis

Statistical analysis was performed using Student's *t*-test for dual comparison and one-way ANOVA for multiple comparison with SigmaPlot 12.0 (Systat Software Inc.). Differences were considered statistically significant if $P<0.05$.

Plasmids and siRNA

pCX-EGFP was a kind gift from Masaru Okabe and Jun-ichi Miyazaki (Osaka University, Osaka, Japan). pCAG-Cre-IRES2-GFP (Woodhead et al., 2006) (Addgene plasmid 26646) was provided by Anjen Chenn (Northwestern University, Evanston, IL). For *in vivo* electroporation, the DNA sequences encoding Myc-tagged human WT RalA, constitutively active (CA) RalA (RalAQ72L), fast cycling (FC) RalA (RalAF39L), and dominant-negative (DN) RalA (RalAS28N) were amplified by PCR from the original constructs in pRK5-myc (Lalli, 2009) using the primers 5′-GAATTGGCTAGCATGGAGCAGAAGCTGATCTCCGAGGAGG-3′ and 5′-TCTGCAGATCGATTTATAAAATGCAGCATCTTTCTCTG-3′, and subcloned into pCAG-IRES-EGFP (a kind gift from M. Hoshino, National Institute of Neuroscience, Tokyo, Japan) (Causeret et al., 2009). The different effector-uncoupled CA RalA versions were obtained from site-directed mutagenesis of pCAG-CARalA-IRES-EGFP using the following primers for Exo84-uncoupled RalAQ72LA48W: 5′-AGGACTATGAG-CCTACCAAATGGGACAGCT/et al/et al/tgciqACCGGAAGAAGG-3′ and 5′-CCTTCTTCGGAGCTGTCCCATTTGGTAGGCTCATAGTCC-T-3′; and for RalBP1-uncoupled RalAQ72LD49N, 5′-GCCTACCAAA-GCAAACAGCTACCGGAAGAAGG-3′ and 5′-CCTTCTTCCGGTAG-CTGTTTGCTTTGGTAGGC-3′.

The Exo84, Par3 and Par6 constructs used for *in vitro* translation, immunoprecipitation and direct binding assays were: pcDNA3.1-Exo84 (1–716); pcDNA3.1-Exo84-CΔ3 (1–713); pcDNA3.1-Exo84-INT-mt (1–716, $V^{348}D{\rightarrow}AA^{349}$); pEGFPC2-Exo84 (1–716); pEGFPC2-Exo84-CΔ3 (1–713); pEGFPC2-Exo84-INT-mt (1–716, $V^{348}D{\rightarrow}AA^{349}$).

Par3-PDZ1, Par3-PDZ2, Par3-PDZ3, Par3-PDZ(2+3) and Par6C-PDZ in pGEX4T-1 (Lin et al., 2000) were kindly provided by Tony Pawson (Samuel Lunenfeld Research Institute, Toronto, Canada).

To generate His_6-tagged Exo84 fusion proteins, the internal Exo84 fragment (INT-frag, aa 251–450) and the Exo84 internal fragment mutant (INT-frag-mt, 251–450 aa; $V^{348}D{\rightarrow}AA^{349}$) were amplified by PCR using primers incorporating appropriate restriction sites, and cloned in frame into pET32a(+) to generate His_6–Exo84-INT-frag and His_6–Exo84-INT-frag-mt. His_6-tagged RalA23V and RalA28N were generated by cloning into pET32a(+). The sequences encoding Exo84 INT-frag and Exo84 INT-frag-mt were inserted into pCAG-IRES-EGFP for *in vivo* electroporation. All constructs were confirmed by DNA sequencing.

For siRNA experiments in rat neuroblasts, we used a validated siRNA oligonucleotide targeting RalA [AGACTACGCTGCAATTAGA (Dharmacon) (Lalli, 2009)]. A non-targeting siRNA oligonucleotide was used as a control (AGGUAGUGUAAUCGCCUUGTT). For rescue experiments we co-nucleofected rat neuroblasts with siRNA oligonucleotides together with either pCAG-IRES-EGFP or with pCAG-wtRalA-IRES-EGFP, which contains an siRNA-resistant version of wild-type simian RalA with two mismatches in the region targeted by the RalA siRNA oligonucleotide.

Immortalized human retinal pigmented epithelial cells (hTERT-RPE1) were grown to 50% confluence and transfected using Lipofectamine 2000 with siRNA duplexes targeting human Exo84 (5′-GGTGCCACTT-TACTCTATA-3′), human RalA (5′-CCAAATGAAGGGATACCAT-3′) and human Sec8 (5′-AGAACCTGCTTTCATGCAA-3′). We used the Luciferase siRNA duplex GL2 (5′-AACGTACGCGGAATACTTCGA-3′) targeting luciferase as a control. The efficiency of protein knockdown was determined by western blotting.

Immunoprecipitation from RMS tissue and from cortical neurons

The RMS from P7 rat pups was carefully dissected and homogenized in 100 µl of immunoprecipitation (IP) buffer containing 150 mM NaCl, 10 mM Tris-HCl pH 7.4, 1 mM EDTA, 1 mM EGTA pH 8.0, 1 mM $MgCl_2$, 1 mM Na_3VO_4, 10 mM NaF, 1 mM PMSF and one Complete protease-inhibitor tablet/10 ml (Roche). After incubating for 30 minutes on ice, homogenates were cleared by centrifugation at 19,280 ***g*** for 15 minutes at 4℃ and pre-cleared for 1 hours with protein-G–Sepharose on a rotating wheel at 4℃. Protein concentration was measured in supernatants using a Bradford assay (Bio-Rad Laboratories). Extracts were then incubated with 2 µg of anti-Sec6 antibody or control IgG and protein-G–Sepharose overnight at 4℃. After centrifugation for 5 minutes at 560 ***g***, immunocomplexes were washed four times with IP buffer containing 250 mM NaCl and 0.5% Triton X-100, eluted in boiling Laemlli sample buffer, and examined by SDS-PAGE and western blot analysis with the indicated antibodies as previously described (Lalli, 2009). A similar protocol was followed to immunoprecipitate Sec6 from embryonic rat cortical neurons nucleofected with either GFP or GFP-Exo84 INT-frag (~23×10^6 cells per IP).

Acknowledgements

We thank Anjen Chenn, Mikio Hoshino, Shu-chan Hsu, Jun-ichi Miyazaki, Masaru Okabe, Tony Pawson and Charles Yeaman for providing reagents and Matt Grubb, Alan Hall and Giampietro Schiavo for valuable comments on the manuscript.

Competing interests

The authors declare no competing interests.

Author contributions

A.D., S.G. and K.F. performed experiments, analyzed data and contributed to manuscript preparation. M.J.O., S.F. and B.W. performed experiments. P.P. and C.J.M. provided mouse genetic models, and contributed to data interpretation and article preparation. P.D. contributed to data interpretation. G.L. and W.G. conceived and designed the experiments and wrote the manuscript.

Funding

This work was supported by a Wellcome Trust Project Grant [grant number 089236/Z/09/Z to P.D. and G.L.]; the National Institutes of Health [grant number GM085146 to W.G.]; and grants from the American Heart Association (to W.G.). A.D. was supported by a National Kidney Foundation post-doctoral fellowship; S.F. is supported by an American Heart Association postdoctoral fellowship; P.P. was supported by EMBO Long-Term and Terry Fox Foundation Canadian Cancer Society fellowships; and C.J.M. is supported by Cancer Research UK. Deposited in PMC for release after 6 months.

Supplementary material

Supplementary material available online at
http://jcs.biologists.org/lookup/suppl/doi:10.1242/jcs.145037/-/DC1

References

Arvidsson, A., Collin, T., Kirik, D., Kokaia, Z. and Lindvall, O. (2002). Neuronal replacement from endogenous precursors in the adult brain after stroke. *Nat. Med.* **8**, 963-970.

Balenci, L., Saoudi, Y., Grunwald, D., Deloulme, J. C., Bouron, A., Bernards, A. and Baudier, J. (2007). IQGAP1 regulates adult neural progenitors in vivo and vascular endothelial growth factor-triggered neural progenitor migration in vitro. *J. Neurosci.* **27**, 4716-4724.

Belvindrah, R., Hankel, S., Walker, J., Patton, B. L. and Müller, U. (2007). Beta1 integrins control the formation of cell chains in the adult rostral migratory stream. *J. Neurosci.* **27**, 2704-2717.

Belvindrah, R., Nissant, A. and Lledo, P. M. (2011). Abnormal neuronal migration changes the fate of developing neurons in the postnatal olfactory bulb. *J. Neurosci.* **31**, 7551-7562.

Bodemann, B. O. and White, M. A. (2008). Ral GTPases and cancer: linchpin support of the tumorigenic platform. *Nat. Rev. Cancer* **8**, 133-140.

Boutin, C., Diestel, S., Desoeuvre, A., Tiveron, M. C. and Cremer, H. (2008). Efficient in vivo electroporation of the postnatal rodent forebrain. *PloS One* **3**, e1883.

Bovetti, S., Bovolin, P., Perroteau, I. and Puche, A. C. (2007). Subventricular zone-derived neuroblast migration to the olfactory bulb is modulated by matrix remodelling. *Eur. J. Neurosci.* **25**, 2021-2033.

Camonis, J. H. and White, M. A. (2005). Ral GTPases: corrupting the exocyst in cancer cells. *Trends Cell Biol.* **15**, 327-332.

Carmena, A., Makarova, A. and Speicher, S. (2011). The Rap1-Rgl-Ral signaling network regulates neuroblast cortical polarity and spindle orientation. *J. Cell Biol.* **195**, 553-562.

Causeret, F., Terao, M., Jacobs, T., Nishimura, Y. V., Yanagawa, Y., Obata, K., Hoshino, M. and Nikolic, M. (2009). The p21-activated kinase is required for neuronal migration in the cerebral cortex. *Cereb. Cortex* **19**, 861-875.

Chen, L., Liao, G., Yang, L., Campbell, K., Nakafuku, M., Kuan, C. Y. and Zheng, Y. (2006). Cdc42 deficiency causes Sonic hedgehog-independent holoprosencephaly. *Proc. Natl. Acad. Sci. USA* **103**, 16520-16525.

Doetsch, F. and Alvarez-Buylla, A. (1996). Network of tangential pathways for neuronal migration in adult mammalian brain. *Proc. Natl. Acad. Sci. USA* **93**, 14895-14900.

Falenta, K., Gajendra, S., Sonego, M., Doherty, P. and Lalli, G. (2013). Nucleofection of rodent neuroblasts to study neuroblast migration in vitro. *J. Vis. Exp.* **81**, e50989.

Farkas, L. M. and Huttner, W. B. (2008). The cell biology of neural stem and progenitor cells and its significance for their proliferation versus differentiation during mammalian brain development. *Curr. Opin. Cell Biol.* **20**, 707-715.

Feng, S., Knödler, A., Ren, J., Zhang, J., Zhang, X., Hong, Y., Huang, S., Peränen, J. and Guo, W. (2012). A Rab8 guanine nucleotide exchange factor-effector interaction network regulates primary ciliogenesis. *J. Biol. Chem.* **287**, 15602-15609.

Fukai, S., Matern, H. T., Jagath, J. R., Scheller, R. H. and Brunger, A. T. (2003). Structural basis of the interaction between RalA and Sec5, a subunit of the sec6/8 complex. *EMBO J.* **22**, 3267-3278.

Goldstein, B. and Macara, I. G. (2007). The PAR proteins: fundamental players in animal cell polarization. *Dev. Cell* **13**, 609-622.

Grindstaff, K. K., Yeaman, C., Anandasabapathy, N., Hsu, S. C., Rodriguez-Boulan, E., Scheller, R. H. and Nelson, W. J. (1998). Sec6/8 complex is recruited to cell-cell contacts and specifies transport vesicle delivery to the basal-lateral membrane in epithelial cells. *Cell* **93**, 731-740.

Guo, W., Grant, A. and Novick, P. (1999). Exo84p is an exocyst protein essential for secretion. *J. Biol. Chem.* **274**, 23558-23564.

Hall, A. and Lalli, G. (2010). Rho and Ras GTPases in axon growth, guidance, and branching. *Cold Spring Harb. Perspect. Biol.* **2**, a001818.

Hazelett, C. C. and Yeaman, C. (2012). Sec5 and Exo84 mediate distinct aspects of RalA-dependent cell polarization. *PLoS ONE* **7**, e39602.

Hazelett, C. C., Sheff, D. and Yeaman, C. (2011). RalA and RalB differentially regulate development of epithelial tight junctions. *Mol. Biol. Cell* **22**, 4787-4800.

He, B. and Guo, W. (2009). The exocyst complex in polarized exocytosis. *Curr. Opin. Cell Biol.* **21**, 537-542.

He, J. C., Gomes, I., Nguyen, T., Jayaram, G., Ram, P. T., Devi, L. A. and Iyengar, R. (2005). The G alpha(o/i)-coupled cannabinoid receptor-mediated neurite outgrowth involves Rap regulation of Src and Stat3. *J. Biol. Chem.* **280**, 33426-33434.

Hertzog, M. and Chavrier, P. (2011). Cell polarity during motile processes: keeping on track with the exocyst complex. *Biochem. J.* **433**, 403-409.

Hitoshi, N., Yamamura, K. and Miyazaki, J. (1991). Efficient selection for high-expression transfectants with a novel eukaryotic vector. *Gene* **108**, 193-199.

Hsu, S. C., Ting, A. E., Hazuka, C. D., Davanger, S., Kenny, J. W., Kee, Y. and Scheller, R. H. (1996). The mammalian brain rsec6/8 complex. *Neuron* **17**, 1209-1219.

Hsu, S. C., TerBush, D., Abraham, M. and Guo, W. (2004). The exocyst complex in polarized exocytosis. *Int. Rev. Cytol.* **233**, 243-265.

Joberty, G., Petersen, C., Gao, L. and Macara, I. G. (2000). The cell-polarity protein Par6 links Par3 and atypical protein kinase C to Cdc42. *Nat. Cell Biol.* **2**, 531-539.

Jossin, Y. and Cooper, J. A. (2011). Reelin, Rap1 and N-cadherin orient the migration of multipolar neurons in the developing neocortex. *Nat. Neurosci.* **14**, 697-703.

Jullien-Flores, V., Mahé, Y., Mirey, G., Leprince, C., Meunier-Bisceuil, B., Sorkin, A. and Camonis, J. H. (2000). RLIP76, an effector of the GTPase Ral, interacts with the AP2 complex: involvement of the Ral pathway in receptor endocytosis. *J. Cell Sci.* **113**, 2837-2844.

Kazanis, I., Lathia, J. D., Vadakkan, T. J., Raborn, E., Wan, R., Mughal, M. R., Eckley, D. M., Sasaki, T., Patton, B., Mattson, M. P. et al. (2010). Quiescence

and activation of stem and precursor cell populations in the subependymal zone of the mammalian brain are associated with distinct cellular and extracellular matrix signals. *J. Neurosci.* **30**, 9771-9781.
Koizumi, H., Higginbotham, H., Poon, T., Tanaka, T., Brinkman, B. C. and Gleeson, J. G. (2006). Doublecortin maintains bipolar shape and nuclear translocation during migration in the adult forebrain. *Nat. Neurosci.* **9**, 779-786.
Lalli, G. (2009). RalA and the exocyst complex influence neuronal polarity through PAR-3 and aPKC. *J. Cell Sci.* **122**, 1499-1506.
Lalli, G. (2013). Extracellular signals controlling neuroblast migration in the postnatal brain. In *New Insights into the Cellular and Molecular Control of Neuron Migration* (ed. L. Nguyen and S. Hippenmeyer), pp. xxx. Xxxx: Springer.
Lalli, G. and Hall, A. (2005). Ral GTPases regulate neurite branching through GAP-43 and the exocyst complex. *J. Cell Biol.* **171**, 857-869.
Letinic, K., Sebastian, R., Toomre, D. and Rakic, P. (2009). Exocyst is involved in polarized cell migration and cerebral cortical development. *Proc. Natl. Acad. Sci. USA* **106**, 11342-11347.
Lim, K. H., Baines, A. T., Fiordalisi, J. J., Shipitsin, M., Feig, L. A., Cox, A. D., Der, C. J. and Counter, C. M. (2005). Activation of RalA is critical for Ras-induced tumorigenesis of human cells. *Cancer Cell* **7**, 533-545.
Lin, D., Edwards, A. S., Fawcett, J. P., Mbamalu, G., Scott, J. D. and Pawson, T. (2000). A mammalian PAR-3-PAR-6 complex implicated in Cdc42/Rac1 and aPKC signalling and cell polarity. *Nat. Cell Biol.* **2**, 540-547.
Liu, J. and Guo, W. (2012). The exocyst complex in exocytosis and cell migration. *Protoplasma* **249**, 587-597.
Liu, J., Yue, P., Artym, V. V., Mueller, S. C. and Guo, W. (2009). The role of the exocyst in matrix metalloproteinase secretion and actin dynamics during tumor cell invadopodia formation. *Mol. Biol. Cell* **20**, 3763-3771.
Lledo, P. M., Alonso, M. and Grubb, M. S. (2006). Adult neurogenesis and functional plasticity in neuronal circuits. *Nat. Rev. Neurosci.* **7**, 179-193.
Lois, C. and Alvarez-Buylla, A. (1994). Long-distance neuronal migration in the adult mammalian brain. *Science* **264**, 1145-1148.
Ludford-Menting, M. J., Oliaro, J., Sacirbegovic, F., Cheah, E. T., Pedersen, N., Thomas, S. J., Pasam, A., Iazzolino, R., Dow, L. E., Waterhouse, N. J. et al. (2005). A network of PDZ-containing proteins regulates T cell polarity and morphology during migration and immunological synapse formation. *Immunity* **22**, 737-748.
Luskin, M. B. (1993). Restricted proliferation and migration of postnatally generated neurons derived from the forebrain subventricular zone. *Neuron* **11**, 173-189.
McCaffrey, L. M. and Macara, I. G. (2009). Widely conserved signaling pathways in the establishment of cell polarity. *Cold Spring Harb. Perspect. Biol.* **1**, a001370.
Mellman, I. and Nelson, W. J. (2008). Coordinated protein sorting, targeting and distribution in polarized cells. *Nat. Rev. Mol. Cell Biol.* **9**, 833-845.
Moskalenko, S., Henry, D. O., Rosse, C., Mirey, G., Camonis, J. H. and White, M. A. (2002). The exocyst is a Ral effector complex. *Nat. Cell Biol.* **4**, 66-72.
Moskalenko, S., Tong, C., Rosse, C., Mirey, G., Formstecher, E., Daviet, L., Camonis, J. and White, M. A. (2003). Ral GTPases regulate exocyst assembly through dual subunit interactions. *J. Biol. Chem.* **278**, 51743-51748.
Munson, M. and Novick, P. (2006). The exocyst defrocked, a framework of rods revealed. *Nat. Struct. Mol. Biol.* **13**, 577-581.
Murase, S. and Horwitz, A. F. (2002). Deleted in colorectal carcinoma and differentially expressed integrins mediate the directional migration of neural precursors in the rostral migratory stream. *J. Neurosci.* **22**, 3568-3579.
Murthy, M., Garza, D., Scheller, R. H. and Schwarz, T. L. (2003). Mutations in the exocyst component Sec5 disrupt neuronal membrane traffic, but neurotransmitter release persists. *Neuron* **37**, 433-447.
Nam, S. C., Kim, Y., Dryanovski, D., Walker, A., Goings, G., Woolfrey, K., Kang, S. S., Chu, C., Chenn, A., Erdelyi, F. et al. (2007). Dynamic features of postnatal subventricular zone cell motility: a two-photon time-lapse study. *J. Comp. Neurol.* **505**, 190-208.
Oudin, M. J., Gajendra, S., Williams, G., Hobbs, C., Lalli, G. and Doherty, P. (2011). Endocannabinoids regulate the migration of subventricular zone-derived neuroblasts in the postnatal brain. *J. Neurosci.* **31**, 4000-4011.
Oxford, G., Owens, C. R., Titus, B. J., Foreman, T. L., Herlevsen, M. C., Smith, S. C. and Theodorescu, D. (2005). RalA and RalB: antagonistic relatives in cancer cell migration. *Cancer Res.* **65**, 7111-7120.
Penkert, R. R., DiVittorio, H. M. and Prehoda, K. E. (2004). Internal recognition through PDZ domain plasticity in the Par-6-Pals1 complex. *Nat. Struct. Mol. Biol.* **11**, 1122-1127.
Peschard, P., McCarthy, A., Leblanc-Dominguez, V., Yeo, M., Guichard, S., Stamp, G. and Marshall, C. J. (2012). Genetic deletion of RALA and RALB small GTPases reveals redundant functions in development and tumorigenesis. *Curr. Biol.* **22**, 2063-2068.
Rossé, C., Hatzoglou, A., Parrini, M. C., White, M. A., Chavrier, P. and Camonis, J. (2006). RalB mobilizes the exocyst to drive cell migration. *Mol. Cell. Biol.* **26**, 727-734.
Rosse, C., Formstecher, E., Boeckeler, K., Zhao, Y., Kremerskothen, J., White, M. D., Camonis, J. H. and Parker, P. J. (2009). An aPKC-exocyst complex controls paxillin phosphorylation and migration through localised JNK1 activation. *PLoS Biol.* **7**, e1000235.
Sakurai-Yageta, M., Recchi, C., Le Dez, G., Sibarita, J. B., Daviet, L., Camonis, J., D'Souza-Schorey, C. and Chavrier, P. (2008). The interaction of IQGAP1 with the exocyst complex is required for tumor cell invasion downstream of Cdc42 and RhoA. *J. Cell Biol.* **181**, 985-998.
Sanai, N., Nguyen, T., Ihrie, R. A., Mirzadeh, Z., Tsai, H. H., Wong, M., Gupta, N., Berger, M. S., Huang, E., Garcia-Verdugo, J. M. et al. (2011). Corridors of migrating neurons in the human brain and their decline during infancy. *Nature* **478**, 382-386.
Schaar, B. T. and McConnell, S. K. (2005). Cytoskeletal coordination during neuronal migration. *Proc. Natl. Acad. Sci. USA* **102**, 13652-13657.
Schwamborn, J. C. and Püschel, A. W. (2004). The sequential activity of the GTPases Rap1B and Cdc42 determines neuronal polarity. *Nat. Neurosci.* **7**, 923-929.
Shipitsin, M. and Feig, L. A. (2004). RalA but not RalB enhances polarized delivery of membrane proteins to the basolateral surface of epithelial cells. *Mol. Cell. Biol.* **24**, 5746-5756.
Solecki, D. J., Govek, E. E., Tomoda, T. and Hatten, M. E. (2006). Neuronal polarity in CNS development. *Genes Dev.* **20**, 2639-2647.
Sonego, M., Zhou, Y., Oudin, M. J., Doherty, P. and Lalli, G. (2013a). In vivo postnatal electroporation and time-lapse imaging of neuroblast migration in mouse acute brain slices. *J. Vis. Exp.* (in press)
Sonego, M., Gajendra, S., Parsons, M., Ma, Y., Hobbs, C., Zentar, M. P., Williams, G., Machesky, L. M., Doherty, P. and Lalli, G. (2013b). Fascin regulates the migration of subventricular zone-derived neuroblasts in the postnatal brain. *J. Neurosci.* **33**, 12171-12185.
Spiczka, K. S. and Yeaman, C. (2008). Ral-regulated interaction between Sec5 and paxillin targets Exocyst to focal complexes during cell migration. *J. Cell Sci.* **121**, 2880-2891.
Sugihara, K., Asano, S., Tanaka, K., Iwamatsu, A., Okawa, K. and Ohta, Y. (2002). The exocyst complex binds the small GTPase RalA to mediate filopodia formation. *Nat. Cell Biol.* **4**, 73-78.
Sundholm-Peters, N. L., Yang, H. K., Goings, G. E., Walker, A. S. and Szele, F. G. (2005). Subventricular zone neuroblasts emigrate toward cortical lesions. *J. Neuropathol. Exp. Neurol.* **64**, 1089-1100.
Teodoro, R. O., Pekkurnaz, G., Nasser, A., Higashi-Kovtun, M. E., Balakireva, M., McLachlan, I. G., Camonis, J. and Schwarz, T. L. (2013). Ral mediates activity-dependent growth of postsynaptic membranes via recruitment of the exocyst. *EMBO J.* **32**, 2039-2055.
TerBush, D. R. and Novick, P. (1995). Sec6, Sec8, and Sec15 are components of a multisubunit complex which localizes to small bud tips in Saccharomyces cerevisiae. *J. Cell Biol.* **130**, 299-312.
TerBush, D. R., Maurice, T., Roth, D. and Novick, P. (1996). The Exocyst is a multiprotein complex required for exocytosis in Saccharomyces cerevisiae. *EMBO J.* **15**, 6483-6494.
Valiente, M. and Marín, O. (2010). Neuronal migration mechanisms in development and disease. *Curr. Opin. Neurobiol.* **20**, 68-78.
Vega, I. E. and Hsu, S. C. (2001). The exocyst complex associates with microtubules to mediate vesicle targeting and neurite outgrowth. *J. Neurosci.* **21**, 3839-3848.
Wichterle, H., Garcia-Verdugo, J. M. and Alvarez-Buylla, A. (1997). Direct evidence for homotypic, glia-independent neuronal migration. *Neuron* **18**, 779-791.
Woodhead, G. J., Mutch, C. A., Olson, E. C. and Chenn, A. (2006). Cell-autonomous beta-catenin signaling regulates cortical precursor proliferation. *J. Neurosci.* **26**, 12620-12630.
Yagita, Y., Sakurai, T., Tanaka, H., Kitagawa, K., Colman, D. R. and Shan, W. (2009). N-cadherin mediates interaction between precursor cells in the subventricular zone and regulates further differentiation. *J. Neurosci. Res.* **87**, 3331-3342.
Zhang, H. and Macara, I. G. (2008). The PAR-6 polarity protein regulates dendritic spine morphogenesis through p190 RhoGAP and the Rho GTPase. *Dev. Cell* **14**, 216-226.
Zhao, C., Deng, W. and Gage, F. H. (2008). Mechanisms and functional implications of adult neurogenesis. *Cell* **132**, 645-660.
Zuo, X., Guo, W. and Lipschutz, J. H. (2009). The exocyst protein Sec10 is necessary for primary ciliogenesis and cystogenesis in vitro. *Mol. Biol. Cell* **20**, 2522-2529.

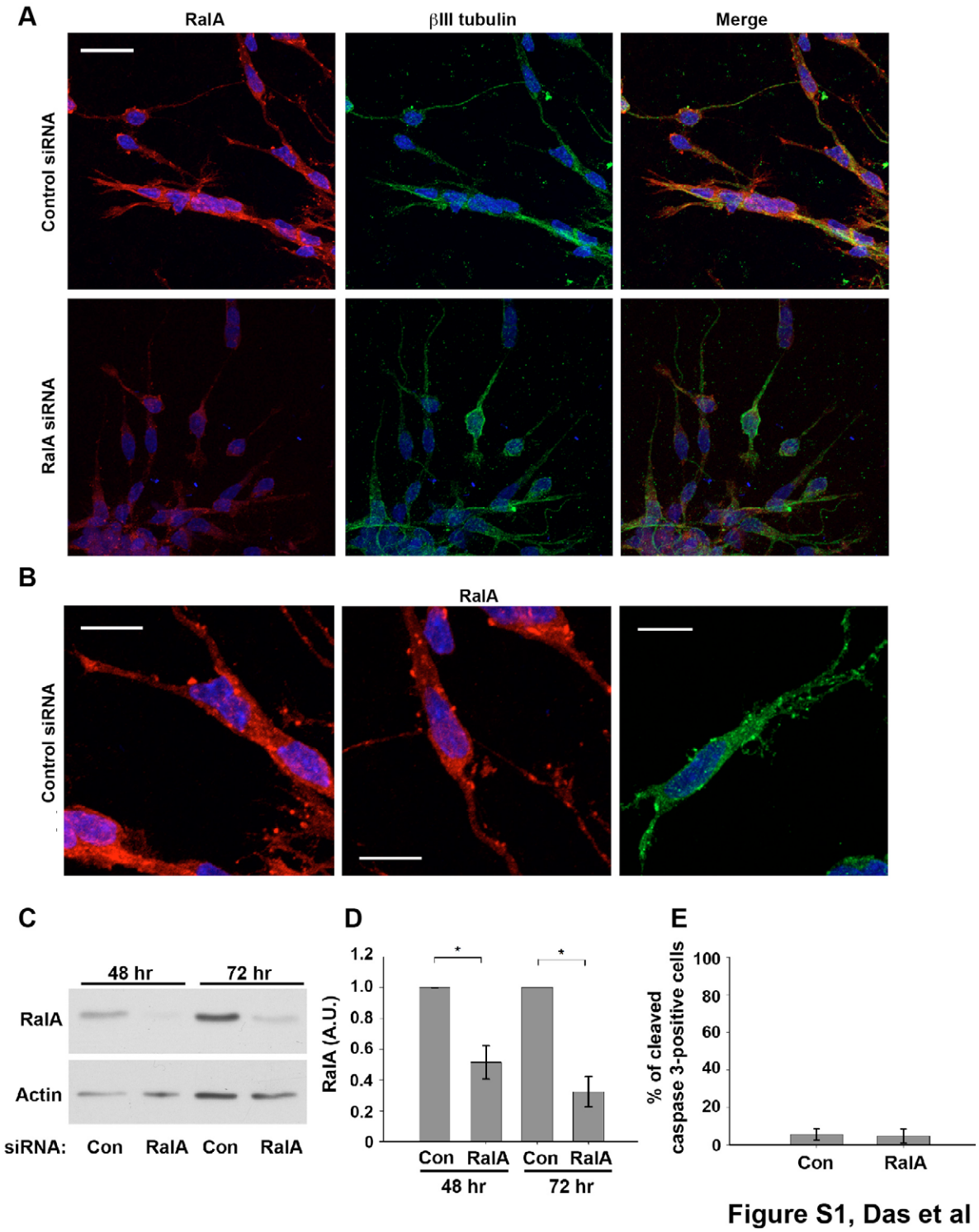

Fig. S1. RalA depletion in RMS neuroblasts. (A) Rat RMS neuroblasts were nucleofected with a control or RalA siRNA oligo and re-aggregated into clusters, embedded in Matrigel 48 h later and allowed to migrate for 24 h before immunostaining for RalA (red) and β III tubulin (green). Cell nuclei (blue) are visualized by Hoechst dye. RalA expression was significantly reduced by the RalA siRNA oligo. Bar, 20 µm. (B) High magnification pictures showing reproducible RalA punctate distribution (red or green) in neuroblasts nucleofected with control siRNA in two different experiments. Cell nuclei (blue) are visualized by Hoechst. Bars, 10 µm. (C) Representative western blot showing reduced expression of RalA at both 48 and 72 h after nucleofection with a RalA siRNA oligo compared to a control (Con) oligo. (D) Densitometric western blot analysis showing significant RalA reduction 48 and 72 h after RalA siRNA nucleofection. Mean ± SEM; *$p < 0.05$; n = 4 independent experiments. (E) Quantification of cleaved caspase 3-positive cells after nucleofection with control or RalA siRNA shows no significant difference in the percentage of cells undergoing apoptosis. Mean ± SEM; n = 3 independent experiments.

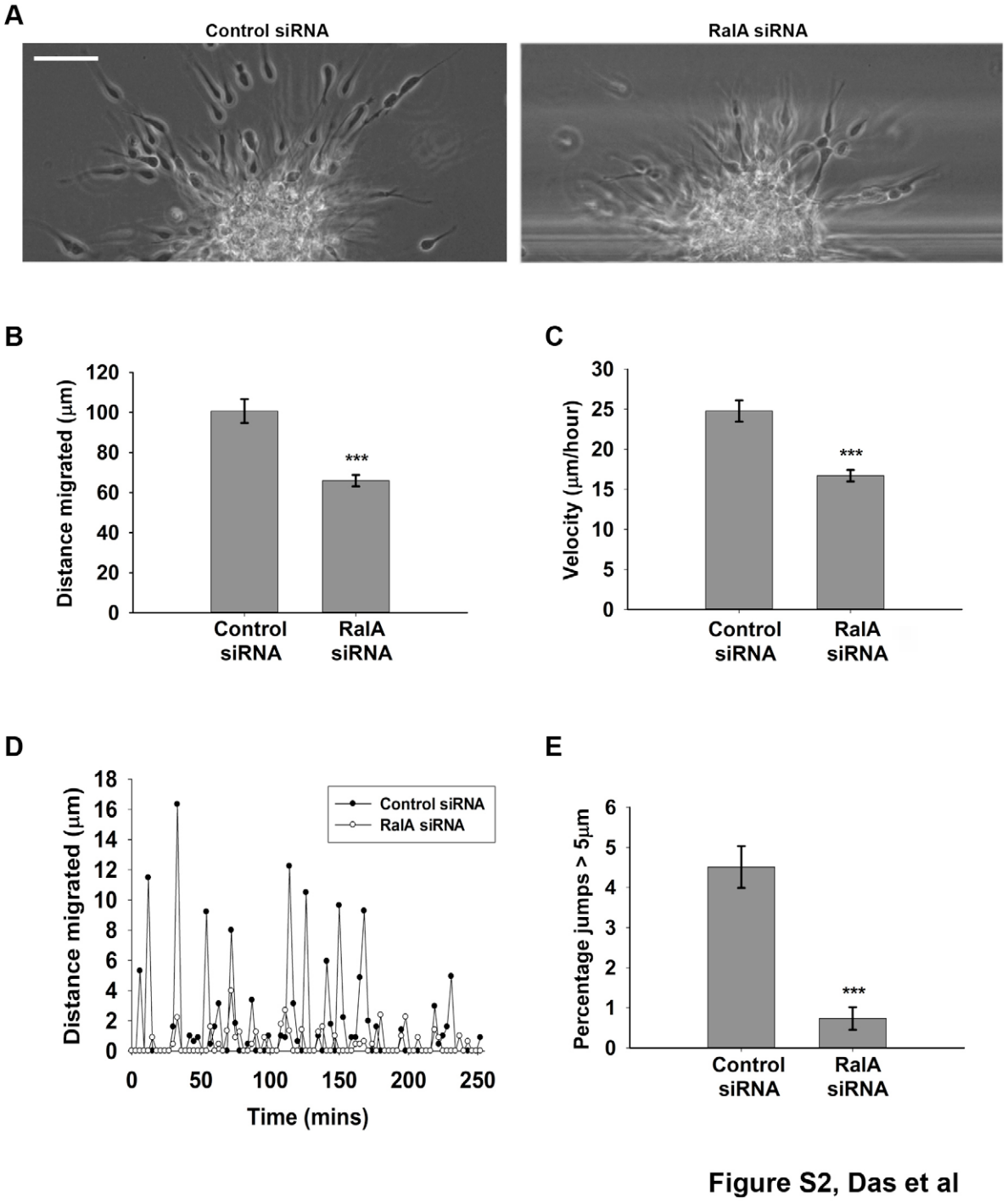

Fig. S2. ***In vitro*** **RalA depletion impairs neuroblast migration.** (A) Snapshots of control and RalA-depleted rat neuroblasts migrating in Matrigel taken 55 h after siRNA nucleofection. Depleting RalA decreased neuroblast migration distance (B) and velocity (C). (D) Representative nuclear displacement traces for control and RalA-depleted neuroblasts. (E) RalA knockdown significantly decreased the percentage of large nuclear jumps. Mean ± SEM; ***$p < 0.001$; for each condition 80 cells were tracked from 3 independent experiments.

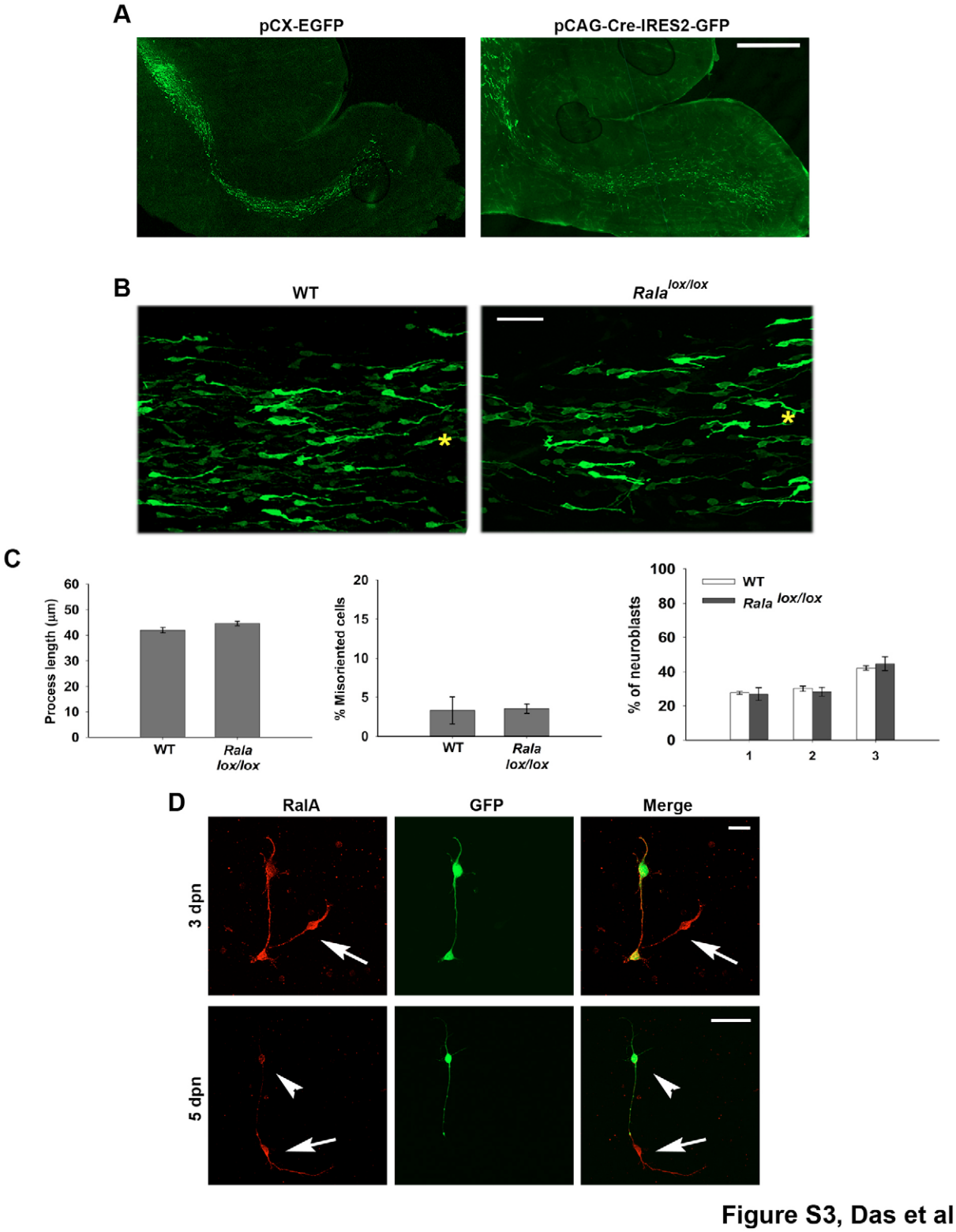

Fig. S3. Cre-induced genetic deletion of *Rala*. (A) Confocal projections of sagittal slices from wt mouse brains immunostained for GFP 5 d after *in vivo* electroporation of pCX-EGFP or pCAG-Cre-IRES2-EGFP. Cre expression *per se* does not affect neuroblast morphology and migration. Bar, 500 µm. (B) wt and *Rala*$^{lox/lox}$ mice were electroporated with pCX-EGFP. Representative confocal projections of fixed RMS sections showing GFP-labeled neuroblasts 5 d after electroporation. Yellow asterisks indicate relative position of the OB. (C) There was no significant difference in process length, orientation, and migration of neuroblasts between wt and *Rala*$^{lox/lox}$ mice. Mean ± SEM; n = 6 brains for wt and *Rala*$^{lox/lox}$. (D) Neuroblasts from P7 *Rala*$^{lox/lox}$ mouse pups were nucleofected with pCAG-Cre-IRES2-GFP, fixed 3 or 5 d later (3dpn/5dpn) and immunostained for RalA (red) and GFP (green). Downregulation of RalA expression is visible in GFP-positive cells only at 5 dpn (arrowhead), while GFP-negative cells retain strong RalA immunoreactivity (arrows). Bars, (3 dpn) 20 µm; (5 dpn) 50 µm.

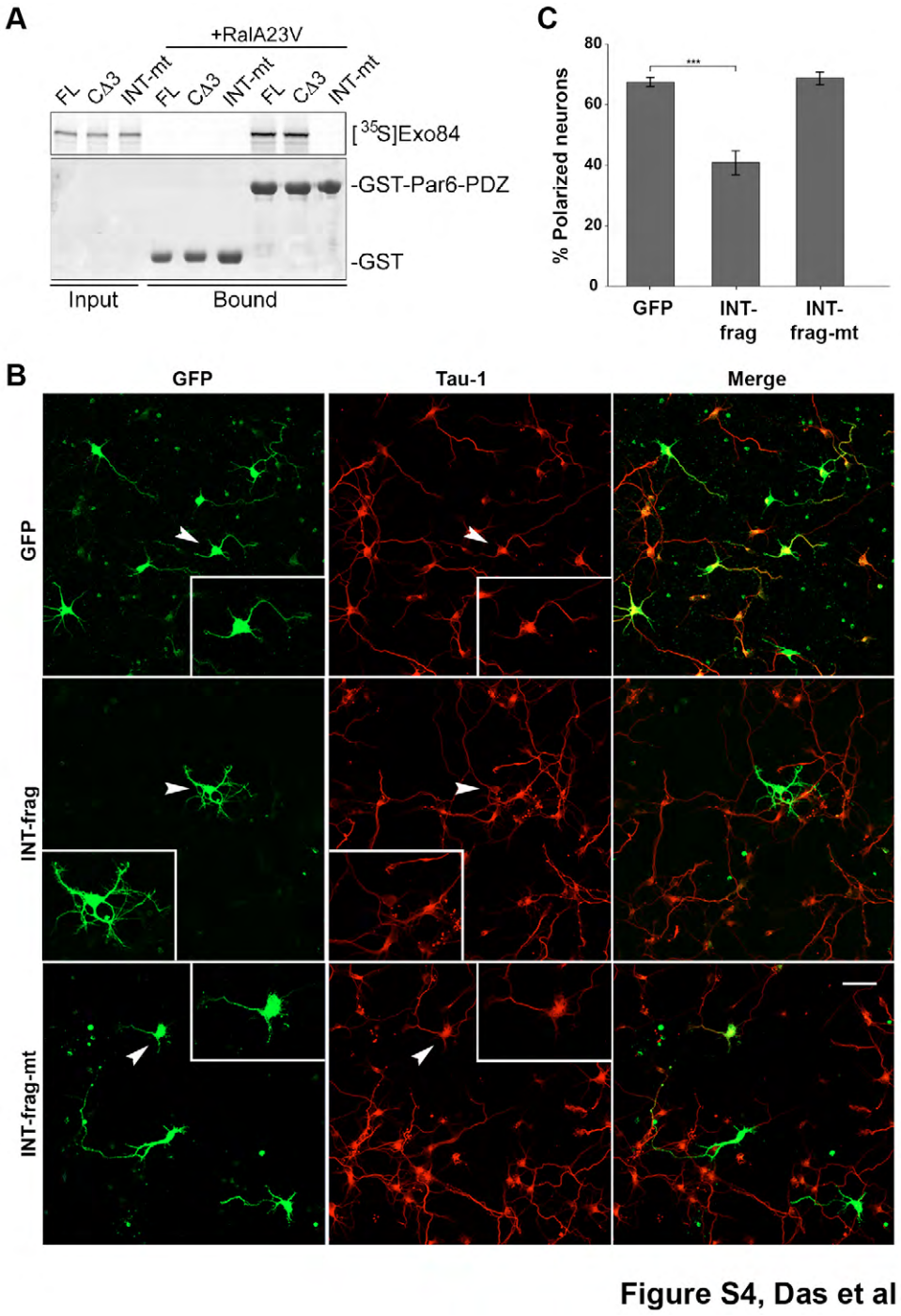

Fig. S4. Disrupting the Exo84-Par6 interaction affects neuronal polarization. (A) The internal PDZ-binding motif of Exo84 is required for RalA-promoted interaction between Exo84 and Par6. *In vitro* translated full length Exo84 (FL), Exo84 lacking the C-terminal PDZ binding domain (CΔ3) and Exo84 mutated in the internal PDZ-binding motif (INT-mt) were incubated with GST-Par6-PDZ in presence of RalA23V. Both Exo84FL and Exo84CΔ3 bound to GST-Par6-PDZ, whereas Exo84INT-mt was unable to interact with Par6-PDZ. The lower panel is a Coomassie blue-stained gel showing the amounts of GST-Par6-PDZ and GST (as control). (B) Embryonic rat cortical neurons were nucleofected with plasmids encoding GFP or GFP-tagged Exo84 fragments and cultured for 48 h before immunostaining for GFP and the axonal marker tau-1. Representative confocal images of neurons nucleofected with the indicated constructs. Most of GFP-labelled control neurons extend a tau-1-positive axon (top row). Expression of GFP-tagged Exo84 INT-frag interacting with Par6-PDZ impairs axonal specification, causing cells to extend minor neurites negative for tau-1 (middle row). Expression of Exo84 INT-frag-mt unable to bind Par6 does not affect neuronal polarization (bottom row). Arrowheads indicate neurons shown at higher magnification in the insets. Bar, 50 µm. (C) Quantitative analysis of neuronal polarization. Mean ± SEM; ***$p < 0.001$; n = 3 independent experiments.